Sensorimotor brain-computer interface performance depends on signal-to-noise ratio but not connectivity of the mu rhythm in a multiverse analysis of longitudinal data

Nikolai Kapralov[a,b,*], Mina Jamshidi Idaji[c,d,a], Tilman Stephani[a,b], Alina Studenova[a], Carmen Vidaurre[e,f,g], Tomas Ros[h,i], Arno Villringer[a,j,k,l], Vadim Nikulin[a,*]

[a] *Department of Neurology, Max Planck Institute for Human Cognitive and Brain Sciences, Leipzig, Germany*
[b] *International Max Planck Research School NeuroCom, Leipzig, Germany*
[c] *BIFOLD — Berlin Institute for the Foundations of Learning and Data, Berlin, Germany*
[d] *Machine Learning Group, Technische Universität Berlin, Berlin, Germany*
[e] *Ikerbasque Science Foundation, Bilbao, Spain*
[f] *TECNALIA, Basque Research and Technology Alliance (BRTA), San Sebastian, Spain*
[g] *Basque Center on Cognition, Brain and Language, Basque Excellence Research Centre (BERC), San Sebastian, Spain*
[h] *Department of Neuroscience and Psychiatry, University of Geneva, Geneva, Switzerland*
[i] *Center for Biomedical Imaging (CIBM), Geneva-Lausanne, Switzerland*
[j] *Charité-Universitätsmedizin Berlin, Berlin, Germany*
[k] *Berlin School of Mind and Brain, Humboldt-Universität zu Berlin, Berlin, Germany*
[l] *Clinic for Cognitive Neurology, University of Leipzig Medical Center, Leipzig, Germany*

Abstract

Serving as a channel for communication with locked-in patients or control of prostheses, sensorimotor brain-computer interfaces (BCIs) decode imaginary movements from the recorded activity of the user's brain. However, many individuals remain unable to control the BCI, and the underlying mechanisms are not clear yet. The user's BCI performance was previously shown to correlate with the resting-state signal-to-noise ratio (SNR) of the mu rhythm and the phase synchronization (PS) of the mu rhythm between sensorimotor areas. Yet, these predictors of performance were primarily evaluated in a single BCI session, while the longitudinal aspect remains rather uninvestigated. In addition, different analysis pipelines were used for the estimation of PS in source space, potentially hindering the reproducibility of the results. To systematically address these issues, we performed an extensive validation of the relationship between pre-stimulus SNR, PS, and session-wise BCI performance using a publicly available dataset of 62 human participants performing up to 11 sessions of BCI training. We combined 24 pipelines for source space analysis and three PS measures in a multiverse analysis to investigate how robust the observed effects were to the selection of the pipeline. Our results show that SNR had a between- and within-subject effect on BCI performance for the majority of the pipelines. In contrast, the effect of phase synchronization on BCI performance was less robust to the selection of the pipeline and became non-significant after controlling for SNR. Taken together, our results demonstrate that changes in neuronal connectivity within the sensorimotor system are not critical for learning to control a BCI, and interventions that increase the SNR of the mu rhythm might lead to improvements in the user's BCI performance.

*Corresponding author
Email addresses: `kapralov@cbs.mpg.de` (Nikolai Kapralov), `nikulin@cbs.mpg.de` (Vadim Nikulin)

1. Introduction

A brain-computer interface (BCI) is a system that decodes the intentions of the user based on the recorded activity of their brain and provides commands to external devices (e.g., prostheses; Wolpaw et al. (2002)). These systems have many potential applications ranging from the clinical ones, such as providing a communication pathway for locked-in patients (Chaudhary et al., 2016), to the research ones, such as the detection of mental states and the facilitation of actions in healthy humans (Blankertz et al., 2010b, 2016). Often, BCIs are based on magnetoencephalographic (MEG) or electroencephalographic (EEG) recordings of brain activity. MEG and EEG (M/EEG) have high temporal resolution and provide multiple features of the ongoing or evoked brain activity that can be used as a control signal (Abiri et al., 2019). For example, BCI paradigms based on the P300 component of the evoked response or steady-state visual evoked responses (SSVEP) provide high information transfer rates for efficient communication (Abiri et al., 2019). However, these paradigms always require external stimuli to be presented, which makes the approach less flexible. In contrast, sensorimotor BCIs decode the imaginary movements of limbs or tongue that can be self-initiated and thus provide more flexibility (Leeb et al., 2007; Yuan and He, 2014; Scherer and Vidaurre, 2018). Decoding of the imaginary movements is often based on the modulation of power in the alpha ($8 - 13$ Hz) and beta ($13 - 30$ Hz) frequency ranges in sensorimotor brain areas, also referred to as event-related desynchronization or synchronization (ERD/ERS; Pfurtscheller and Lopes da Silva (1999); Pfurtscheller et al. (1996)). Sensorimotor BCIs are also used to facilitate the recovery of motor functions during rehabilitation after a stroke (Cervera et al., 2018; Kruse et al., 2020; Peng et al., 2022).

While BCI seems to be a promising approach with multiple clinical applications, some participants remain unable to control it (Allison and Neuper, 2010). Typically, participants complete several training sessions to learn to control a BCI. However, their performance in the task varies considerably, and on average around 20% of the participants fail to learn the task (Sannelli et al., 2019). The mechanisms underlying successful modulation of brain activity for controlling a BCI are not clear yet. However, previous studies have identified several psychological (Hammer et al., 2012; Jeunet et al., 2015) and neurophysiological (Blankertz et al., 2010a; Sugata et al., 2014; Samek et al., 2016; Vidaurre et al., 2020) predictors of successful control of a sensorimotor BCI. These predictors allow pre-screening of participants in order to provide the full training only if the participant is likely to be successful in controlling the BCI (Sannelli et al., 2019).

Neurophysiological predictors of successful BCI control also provide information about the features of brain activity (e.g., neuronal networks) that play a role in the success of BCI training. For example, the signal-to-noise ratio (SNR) of the sensorimotor mu rhythm during resting-state was positively correlated ($r = 0.53$) with online accuracy of sensorimotor BCI control (Blankertz et al., 2010a). This predictor was later validated in an independent dataset with a similar experimental paradigm (Acqualagna et al., 2016). Moreover, several other neural correlates of performance in a sensorimotor BCI task are related to the SNR of the mu rhythm, for example, the performance potential factor (Ahn et al., 2013) or the spectral entropy at C3 electrode during resting-state (Zhang et al., 2015). Although SNR seems to be a well-established predictor of BCI performance, it is often investigated in the context of a single BCI session. However, the relationship between SNR and performance could change if participants with low SNR eventually learned the task or if the SNR itself changed throughout a multi-session BCI training. Therefore, it is crucial to validate this predictor in a longitudinal analysis, which is one of the aims of the current study.

Other predictors of sensorimotor BCI performance include long-range temporal correlations (Samek et al., 2016) and functional connectivity between sensorimotor brain regions (Sugata et al., 2014; Vidaurre et al., 2020). Connectivity-based predictors might be especially relevant

since motor imagery involves activation of multiple interacting brain areas (Solodkin et al., 2004; Halder et al., 2011; Hardwick et al., 2018). The strength and the phase lag of these interactions can be quantified using various connectivity measures and then related to the performance in the sensorimotor BCI task. Thereby, connectivity could provide additional information about the underlying neuronal networks that is not reflected in the SNR.

When considering M/EEG-based functional connectivity within the same (e.g., alpha/mu) frequency band, phase synchronization (PS) and amplitude envelope correlation (AEC) can reflect different properties of the underlying neuronal networks. Studies combining EEG and fMRI (functional Magnetic Resonance Imaging) have previously shown that the power of alpha and beta oscillations at C3 and C4 is negatively correlated with the blood-oxygen-level-dependent (BOLD) fMRI signal in sensorimotor areas during the execution of real and imaginary hand movements (Ritter et al., 2009; Yuan et al., 2010). Therefore, AEC primarily captures the low-frequency (below 0.1 Hz) dynamics of brain activity similar to the fMRI connectivity based on the BOLD signal (Engel et al., 2013). In contrast, phase synchronization between high-frequency (above 5 Hz) oscillations might reveal additional information that is only accessible with the high temporal resolution of M/EEG (Engel et al., 2013). In particular, phase synchronization was proposed to be a mechanism of efficient communication between neuronal populations (Engel et al., 2001; Fries, 2005; Palva and Palva, 2007) and can reflect short-term changes in the functional organization of neuronal networks due to plasticity (Engel et al., 2013). Therefore, in the current study, we also investigated the role of phase synchronization of the sensorimotor mu (9-15 Hz) oscillations in the successful control of a sensorimotor BCI.

Several studies have already applied various M/EEG-based phase synchronization measures in the context of sensorimotor BCI training. First, BCI performance was positively correlated with the imaginary part of coherency (ImCoh; Nolte et al. (2004)) of the mu rhythm between sensorimotor areas both before and during the trial (Sugata et al., 2014; Vidaurre et al., 2020). In addition, the phase locking value (PLV; Lachaux et al. (1999)) of alpha-band oscillations within the motor areas of the right hemisphere was higher for the successful participants in comparison to the unsuccessful ones (Leeuwis et al., 2021). Finally, in a whole-head analysis Corsi et al. (2020) observed a global decrease in ImCoh during motor imagery as compared to resting-state. While phase synchronization seems to play a role in sensorimotor BCI training, the results were obtained using various PS measures and partially in the context of single-session experiments. To address these issues, we examined several PS measures and ran a longitudinal analysis of changes in phase synchronization and its relationship with the BCI performance.

Studies investigating longitudinal changes in phase synchronization are scarce in the sensorimotor BCI literature. On the one hand, Corsi et al. (2020) observed a progressive decrease of ImCoh during motor imagery in alpha and beta bands along sessions. On the other hand, the positive correlation between ImCoh and BCI performance in one session (Sugata et al., 2014; Vidaurre et al., 2020) may suggest the entrainment of task-relevant networks throughout the training. However, in both cases, ImCoh reflects a mixture of the strength and the phase lag of the interaction between brain areas, which can only be disentangled with other PS measures, such as coherence. Therefore, further validation of these results in the longitudinal setting with multiple PS measures is necessary.

In practice, the estimation of phase synchronization in M/EEG critically depends on the proper control for confounding factors (Bastos and Schoffelen, 2015). In the current study, we focused on the effects of volume conduction and signal-to-noise ratio (SNR). To overcome these challenges, we used PS measures, which are insensitive to zero-lag interactions (e.g., ImCoh), and applied a correction for SNR in the statistical analysis.

Furthermore, to obtain a higher spatial specificity of the estimated PS values, we performed the source space analysis using time courses of brain activity in particular regions of interest

(ROIs). For this purpose, two-step processing pipelines are typically used (Schoffelen and Gross, 2009). First, inverse modeling is applied to reconstruct time courses of activity for individual sources within the cortex. Second, time courses of activity for all sources within the ROI are aggregated to extract one or several time courses of activity in the ROI. While multiple approaches exist for inverse modeling and extraction of ROI time series, there is no consensus on the most appropriate pipeline in the community. Previous studies have shown that the choice of methods for inverse modeling and extraction of ROI time series affects the estimated PS values in real and simulated data (Mahjoory et al., 2017; Pellegrini et al., 2023). Therefore, multiple pipelines should be considered simultaneously to arrive at a valid conclusion about genuine neuronal connectivity based on M/EEG data.

To address the multitude of possible pipelines while analyzing SNR and phase synchronization as predictors of BCI performance, we ran a multiverse analysis (Steegen et al., 2016) using several pipelines for extraction of ROI time series. While results are typically reported only for one or a few of many possible pipelines, the idea of the multiverse analysis is to consider a set of reasonable pipelines and report the results from all of the considered options. This way, one can not only analyze the variability of the estimated PS values similar to Mahjoory et al. (2017) but also assess the robustness of the observed effects (e.g., on BCI performance) to the selection of the pipeline. More pronounced effects should be more robust to changes in the processing pipeline, and including several pipelines in the analysis may reveal important information about the influence of different processing steps on the observed results.

Overall, in the current study, we aimed to validate and extend the findings about the effects of SNR and phase synchronization of the mu rhythm on BCI performance in a publicly available longitudinal dataset (Stieger et al., 2021). We focused on four sensorimotor ROIs corresponding to the primary motor and somatosensory cortices. These ROIs were previously shown to be the most involved in the BCI training based on imaginary movements (Samek et al., 2016; Vidaurre et al., 2020; Nierhaus et al., 2021). In the current analysis, we aimed to address the following research questions:

1. Do SNR and PS predict performance not just in one but also in multiple training sessions?
2. Do SNR and PS change over time due to BCI training?
3. Are SNR, PS, and the observed effects for questions 1 and 2 robust to the selection of processing steps in the source space analysis?

To touch upon the open questions regarding the multitude of existing approaches for source space analysis and estimation of phase synchronization, we considered a set of existing methods and performed a multiverse analysis to capture the between-pipeline variability in estimated values of SNR and PS, their effects on BCI performance, and longitudinal changes over time. In addition, to ensure the end-to-end repeatability of the results, we designed the analysis pipeline to automatically include the results in a publishable report, which, as we hope, will be useful as a template for future studies involving a multitude of different analysis pipelines.

2. Materials and Methods

2.1. Description of the Dataset

We used publicly available EEG recordings of 62 participants (50 female; 55 right-handed; mean age = 39.2 years, SD = 14.1 years) from a study that investigated the effects of mindfulness-based training on performance in a motor imagery BCI task (Stieger et al., 2021). Participants first completed a baseline BCI training session and then were randomly assigned to an 8-week mindfulness intervention (n = 33; 26 female; 28 right-handed; mean age = 42.2, SD = 14.7) and a wait-list control condition of the same length (n = 29; 24 female; 27 right-handed; mean age

= 35.8, SD = 12.9). After eight weeks, participants returned to the lab for 6-10 more sessions of BCI training (Fig. 1A). All experiments were approved by the institutional review boards of the University of Minnesota and Carnegie Mellon University. Informed consent was obtained from all participants.

2.2. Experimental Procedure

During each BCI session, participants performed imaginary movements (opening and closing) of their hands to control a cursor, which was displayed on the screen in front of them in the BCI2000 system (Schalk et al., 2004). Each session included three tasks: (1) horizontal cursor control task (via imaginary movements of the left or right hand), (2) vertical cursor control task (down: voluntary rest, up: imaginary movement of both hands), (3) 2D control task (the targets were reachable through one of the previous strategies, but the cursor moved in both directions). Each task included 150 trials, and the number of trials was balanced across classes for both 1D and 2D control tasks. In the current study, we only analyzed the data from the first (horizontal cursor control) task.

The structure of all trials is shown in Fig. 1B. First, participants saw a blank screen during the inter-trial interval of 2 s. Then, a bar appeared on one of the sides of the screen, indicating the target action to execute. After 2 seconds of target presentation, a cursor (circle) appeared in the middle of the screen, and its position was calculated based on the EEG data acquired in real time. Trials ended either when the cursor reached any side of the screen (not necessarily the target one) or after the timeout when 6 seconds passed without any target being reached.

Feedback was presented with a cursor, whose position was updated in real time based on the EEG power in the mu (9-15 Hz) frequency range. Power was calculated based on an autoregressive model of order 16 fitted to the most recent 160 ms of the EEG data after applying small Laplacian transform to channels C3 and C4 (using the closest neighboring channels FC3, CP3, C1, C5 and FC4, CP4, C2, C6, respectively). The horizontal position of the cursor was determined by the lateralization of mu power (C4 – C3), while the vertical position reflected the total mu power (C4 + C3). Feedback values were re-calculated every 40 ms and normalized by subtracting the mean and dividing over the standard deviation. The mean and the standard deviation were constantly updated based on the last 30 seconds of data. More details about the experimental procedure can be found in (Stieger et al., 2021).

2.3. EEG Acquisition

EEG was acquired using SynAmps RT amplifiers and Neuroscan acquisition software (Compumedics Neuroscan, VA). Data were recorded with a sampling frequency of 1 kHz and band-pass filtered between 0.1 and 200 Hz with an additional notch filter at 60 Hz. EEG data were acquired from 62 channels with the following locations according to the 10-5 system: Fp1, Fpz, Fp2, AF3, AF4, F7, F5, F3, F1, Fz, F2, F4, F6, F8, FT7, FC5, FC3, FC1, FCz, FC2, FC4, FC6, FT8, T7, C5, C3, C1, Cz, C2, C4, C6, T8, TP7, CP5, CP3, CP1, CPz, CP2, CP4, CP6, TP8, P7, P5, P3, P1, Pz, P2, P4, P6, P8, PO7, PO5, PO3, POz, PO4, PO6, PO8, CB1, O1, Oz, O2, CB2. AFz was used as the ground electrode, while the reference electrode was located between Cz and CPz.

2.4. Preprocessing

EEG preprocessing and analyses were performed in MATLAB R2022b (The MathWorks; RRID: SCR_001622) using custom scripts employing functions from EEGLAB 2021.0 (Delorme and Makeig (2004); RRID: SCR_007292), BBCI (Blankertz et al., 2016), Brainstorm (Tadel et al. (2011); RRID: SCR_001761), MVGC (Barnett and Seth (2014); RRID: SCR_015755) and METH (Guido Nolte; RRID: SCR_016104) toolboxes. For source space visualizations, we utilized functions from (Haufe and Ewald, 2019).

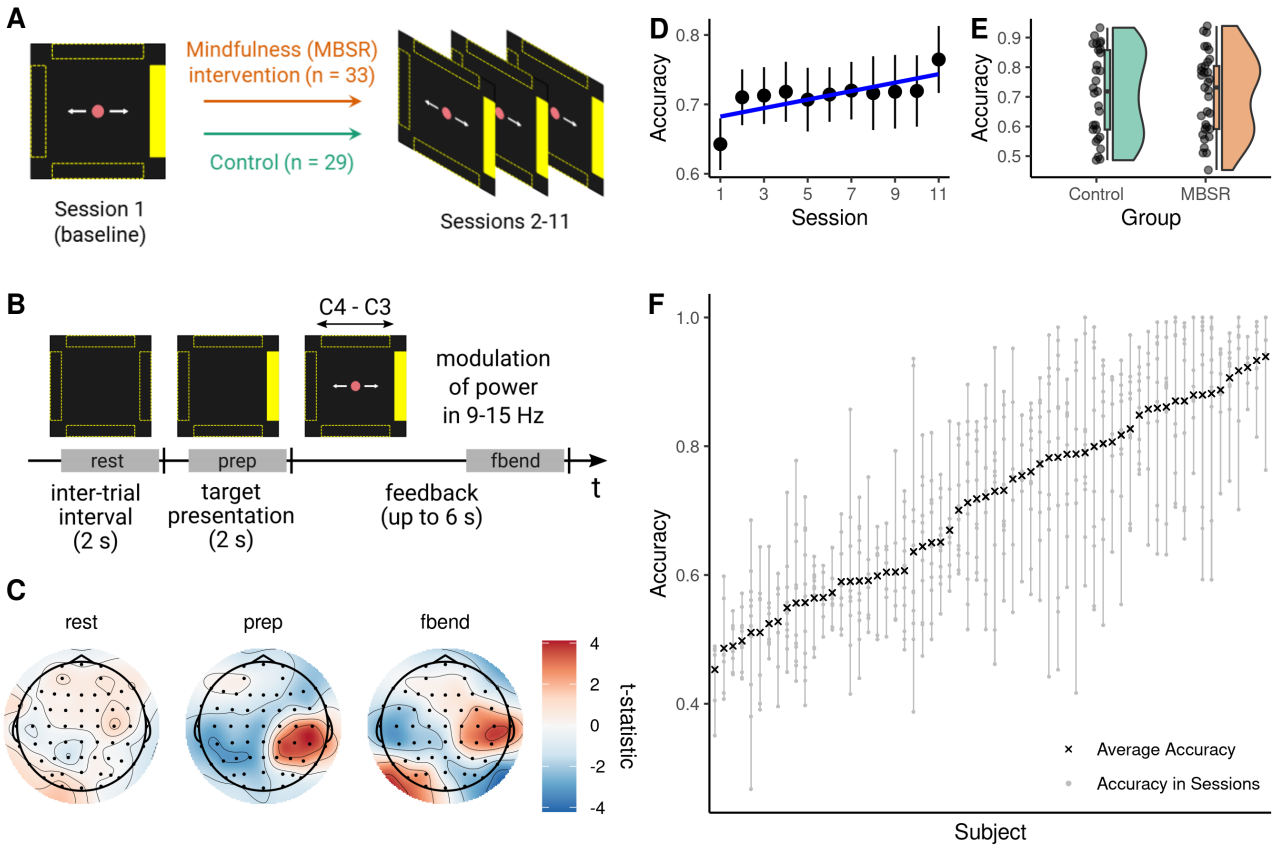

Figure 1: Overview of the publicly available dataset from (Stieger et al., 2021): structure of the BCI training and performance of the participants. (A) Participants were assigned to MBSR (mindfulness-based stress reduction) and control groups and completed up to 11 sessions of cursor control training. (B) Trial structure of the horizontal cursor control task with time windows of interest highlighted. Participants performed imaginary movements of their left and right hands to control a cursor, whose position was calculated based on the values of mu power at Laplace-transformed channels C3 and C4 in real time. (C) Channel-wise t-statistic of difference in mu power between trials that involved imaginary movements of the right and left hand. While no difference in mu power was observed during the resting-state period, effects emerged over sensorimotor areas during target presentation, accompanied by effects over visual areas due to the movement of the cursor during the feedback period. (D) Dynamics of group-average performance reflect improvement over the course of the training. Error bars reflect the standard error of the mean. (E) No difference in average performance in the horizontal cursor control task was observed between groups. (F) High variability of performance in the individual sessions was observed and accounted for in the analyses. Subjects are ordered according to their average accuracy. Vertical bars depict subject-specific ranges of accuracy.

First, trials were concatenated to restore continuous segments of data accounting for breaks during the recording. Then, EEG time series were downsampled to 250 Hz, and channels CB1 and CB2 were removed as they are not part of the 10-10 system. A semi-automatic identification of bad trials, channels, and components was applied as follows. Trials and channels were rejected if the z-score of power within 1-45 Hz was higher than three in at least 5% of trials for a certain channel or in at least 5% of channels for a certain trial. This procedure was performed recursively until nothing could be rejected. Additionally, we used the clean_rawdata EEGLAB plugin to reject channels if one of the following conditions was met: (1) the variance of the channel data was near zero for at least five seconds, (2) the ratio of the power of the line noise and power of the signal below 50 Hz exceeded 4, or (3) the correlation of the channel data with an interpolated estimate based on the data from neighboring channels was less than 0.8. After the removal of bad trials and channels, EEG data were re-referenced to the common average reference and filtered with a forward-backward second-order high-pass Butterworth filter with a cutoff frequency of 1 Hz. Then, we applied independent component analysis (ICA) based on the FastICA approach (Hyvärinen, 1999) and used ICLabel (Pion-Tonachini et al., 2019) for distinguishing ICA components of different types: brain, muscle, eye, heart, line noise, and channel noise. Based on the output of ICLabel, components that explained 95% of the variance in the data were rejected if their probability of originating from the brain was less than 20%, and other components were rejected only if their probability of belonging to one of the non-brain classes was at least 80%.

Results of the automatic preprocessing were verified through visual inspection of power spectra in sensor space as well as topographic maps and power spectra of kept and rejected ICA components. Overall, 3 sessions were excluded from analysis due to poor data quality. Then, we removed previously identified bad trials, channels, and ICA components from the raw EEG data that were not high-pass filtered. The removed channels were interpolated, and EEG time series were downsampled to 250 Hz. DC offset was removed by subtracting the mean of the signal within continuous data segments. The resulting data were used for the analyses described below.

2.5. Overview of the Analyses

In this section, we provide a brief overview of the performed analyses. The detailed description of the processing steps is presented in the subsequent sections.

In the current study, we only analyzed the data from the first (horizontal cursor control) task, which was based on the imaginary movements of the left or right hand. Additionally, we combined the data from both participant groups since a previous analysis of the same dataset has shown that the mindfulness intervention did not affect the performance in the horizontal cursor control task (Stieger et al., 2020).

We estimated the values of SNR of the mu rhythm (in sensor and source space) and phase synchronization between sensorimotor areas (source space only) in order to investigate their relationship with BCI performance and changes over time. For both of the analyses, we focused on the same [0.49, 1.99] s window of the inter-trial interval (labeled as rest in Fig. 1B). During this interval, participants did not perform any task similar to a typical resting-state recording. Previous studies often used resting-state data to predict BCI performance in subsequent training sessions. Additionally, we investigated differences in mu power during the [0.49, 1.99] s window of the target presentation interval as well as the [-1.51, -0.01] s window relative to the end of the feedback interval (Fig. 1C). The performance in the BCI task (later referred to as accuracy) was assessed with the percentage of correct trials among those that did not end due to timeout. Trials were considered correct if the cursor reached the target side of the screen.

In the sensor space analysis, we applied the small Laplacian transform by subtracting the mean of the neighboring channels (FC3, C5, C1, CP3 or FC4, C6, C2, CP4) from data at channels C3 and C4. The same transform was used during the experiment for calculating the feedback values in real time. Then, we estimated the SNR of the mu rhythm (9-15 Hz) and correlated it with the BCI performance similar to (Blankertz et al., 2010a). Additionally, we examined longitudinal changes in SNR across sessions to find out whether the BCI training affected the SNR of the mu rhythm.

In the source space analysis, we estimated the SNR of the mu rhythm and phase synchronization between the sensorimotor regions of interest (ROIs) to obtain higher spatial specificity. The time courses of activity in each ROI were computed through inverse modeling and subsequent aggregation of reconstructed time series of source dipoles within the ROI. Various methods for inverse modeling and extraction of ROI time series are used in the literature with few guidelines for preferring one over the other. Therefore, we combined several widely used data-driven and data-independent approaches in a multiverse analysis (Steegen et al., 2016) to investigate the robustness of SNR and PS values as well as related statistical effects (e.g., on BCI performance) to the selection of the pipeline (Fig. 2A).

2.6. Forward Model

We used the "New York Head" forward model (Huang et al., 2016), which was derived using the finite element method based on the ICBM152 anatomical template (Fonov et al., 2009, 2011). The model contains several lead field matrices calculated for different numbers and orientations of the source dipoles (later referred to as sources). We used the lead field matrix for 4502 sources with fixed orientations perpendicular to the cortical surface. Since channels PO5 and PO6 were not included in the precomputed lead field, we excluded them before source space analysis. The common average reference transform was applied to the lead field matrix to match the preprocessing of the EEG data.

2.7. Inverse Modeling

We used two inverse solutions with different underlying assumptions: eLORETA (Pascual-Marqui, 2007) and linearly constrained minimal variance (LCMV) beamformer (Van Veen et al., 1997). For both approaches, we used the implementation from the METH toolbox (Guido Nolte; RRID: SCR_016104) with minor modifications from (Haufe and Ewald, 2019). The regularization parameter was set to 0.05 and the identity matrix was used as the noise covariance matrix.

eLORETA is a data-independent approach that belongs to the family of weighted minimum norm inverse solutions and provides zero source localization error (Pascual-Marqui et al., 2011). In the described setting, this approach is also data-independent. In contrast, LCMV is a data-driven method and is fit to the covariance matrix of the data. We averaged covariance matrices for both imaginary movements and calculated a separate LCMV beamformer for each subject and session.

2.8. Extraction of ROI Time Series

After the inverse modeling, one obtains a reconstructed time series of activity for each source. Taking into account the spatial resolution of EEG, it is reasonable to reduce the dimensionality of the source space. The common approach is to aggregate time courses of activity of sources within each ROI into a single or several time series. Yet, multiple aggregation methods exist in the literature, and there is no consensus in the community on the most appropriate method. In particular, previous studies have used averaging (Babiloni et al., 2005), averaging with sign flip (AVG-F; Lai et al. (2018)), singular value decomposition (SVD; Rubega et al. (2019)),

etc. In the current analysis, we considered AVG-F and SVD to compare data-independent and data-driven approaches.

For both approaches, the time series of activity for all sources within the ROI are concatenated to form a matrix. By fitting SVD, one decomposes the multivariate time series of activity into components sorted by the explained variance of the reconstructed source data. Then, a few first components are selected to represent the activity of the whole ROI. We considered either only the first (1SVD) or the first three components (3SVD) as, e.g., in (Rubega et al., 2019; Pellegrini et al., 2023) or (Vidaurre et al., 2020; Pellegrini et al., 2023), respectively.

Alternatively, AVG-F assigns equal weights to all sources within the ROI, and a sign flip is applied to some sources to prevent the cancellation of the activity of dipoles with opposite orientations. To determine the sources that should be flipped, SVD is applied to the leadfield of sources within the ROI to find the dominant orientation of source dipoles. If the angle between the orientation of the dipole and the dominant orientation is larger than 90 degrees, the time series corresponding to this dipole is flipped (that is, multiplied by a negative one). We used the implementation of sign flip from Brainstorm (Tadel et al., 2011). Fig. 2C shows 1SVD and AVG-F weights for all sources within the sensorimotor ROIs based on the data of an exemplary subject.

2.9. Anatomical and Task-Based Definitions of ROIs

All the analyses in the source space were performed for four sensorimotor ROIs — pre- and postcentral gyri of both hemispheres — either according to their definitions in the Harvard-Oxford atlas (Frazier et al., 2005; Desikan et al., 2006; Makris et al., 2006; Goldstein et al., 2007; Jenkinson et al., 2012) or reduced to a group of task-relevant sources (Fig. 2B). To select a subset of sources that contribute the most to the observed task-related changes in the brain activity, we applied a mask in source space derived from the common spatial pattern (CSP) transformation (Koles et al., 1990; Ramoser et al., 2000). CSP was applied to the sensor space data filtered in the 9-15 Hz range for extracting spatial filters that explain the most difference in EEG power between the two imaginary movements. For this purpose, we used the EEG data during the [0.49, 1.99] s window of the target presentation interval (labeled as prep in Fig. 1B). Covariance matrices of the signal were calculated for each subject, session, and imaginary movement separately. Then, for each subject and session, covariance matrices corresponding to different imaginary movements were normalized to make the trace of their average equal to one. The normalization allowed us to exclude the difference in signal power between subjects and sessions while preserving the within-session difference in power between channels and imaginary movements. Normalized covariance matrices were averaged over all subjects and sessions and then used to obtain one set of CSP filters and patterns for all participants. CSP patterns were then source reconstructed with eLORETA. A threshold based on 97.5th percentile of activity strength was applied to select the most responsive sources, which formed the resulting source mask. The mask was applied to the anatomical definitions of sensorimotor ROIs to obtain a task-based reduced representation.

2.10. Filtering

Due to the 1/f shape of the M/EEG power spectra, lower frequencies (< 7 Hz) might have higher power and overshadow mu oscillations in covariance calculations. By filtering the data in a narrow frequency band, one makes sure that data-dependent methods (LCMV, SVD) are not affected by frequencies outside of the target band. At the same time, data-independent methods (eLORETA, AVG-F) are not affected by filtering.

To investigate how filtering in a narrow frequency band affects data-dependent methods for inverse modeling and extraction of ROI time series, we considered two cases: broadband with

no filtering (BB) or band-pass filtering in the 9-15 Hz band (NB). A forward-backward fourth-order Butterworth filter was applied before restricting the data to the time windows of interest and applying the inverse modeling. Since the recording contained breaks, 8 seconds of data in the beginning and the end were mirrored to minimize filtering-related artifacts at the edges of continuous data segments. Separate LCMV beamformers and sets of SVD weights were calculated for broadband and narrowband data.

2.11. SNR

SNR was estimated as the ratio of the total power and the power of the aperiodic component of the signal in the 9-15 Hz frequency range as follows:

$$\text{SNR [dB]} = 10 \cdot \log_{10} \frac{P_{total}}{P_{aperiodic}} \tag{2.1}$$

The aperiodic component of the signal was estimated using FOOOF (Fig. 2D; Donoghue et al. (2020)) with the following set of parameters: 1-45 Hz fit range, 2-12 Hz as limits of peak width, and 3 as the maximal number of peaks. Since it is not possible to fit an aperiodic component for the data that was already band-pass filtered in a narrow frequency range, values of SNR for pipelines that involved filtering were copied from the corresponding broadband pipeline, which had all the other steps unchanged. Values of SNR were estimated in the same manner for the sensor space data after the Laplacian transform and in the source space, later referred to as Laplace SNR and ROI SNR, respectively.

2.12. Phase Synchronization

To estimate phase synchronization between time series of activity in ROIs, we employed three measures: imaginary part of coherency (ImCoh; Nolte et al. (2004)), lagged coherence (LagCoh; Pascual-Marqui et al. (2011)), and coherence (the absolute value of coherency). ImCoh and LagCoh are insensitive to all zero-lag interactions, including the spurious ones caused by the volume conduction. However, it may be hard to interpret correlations between performance and phase synchronization as measured by ImCoh and LagCoh. Both measures depend on the strength and the phase lag of the interaction between neuronal populations. If ImCoh or LagCoh is correlated with performance, it is not entirely clear whether the strength or the phase lag of interaction drives the correlation. At the same time, coherence is supposed to solely reflect the strength of an interaction, but is prone to the effects of volume conduction and might be spurious. To combine interpretability and robustness to spurious zero-lag interactions, we have considered all of these PS measures and looked at whether the observed effects are consistent between them.

We computed the phase synchronization via the Fourier transform for broadband pipelines using the Hamming window and 1.5 s segments from different trials (frequency resolution = 0.67 Hz) and averaged the absolute values of PS measures across frequencies of interest (9-15 Hz). If the data were filtered in the 9-15 Hz range, we calculated the phase synchronization via the analytic signal obtained using the Hilbert transform. These approaches were shown to have a negligible difference within the frequency band of interest for Gaussian distributed data (Nolte et al., 2020). In the case of several SVD components per ROI, PS values were first computed for each pair of the SVD components, then the absolute values of PS were averaged. Furthermore, absolute PS values were averaged over within-hemisphere and across-hemisphere edges as shown in Fig. 2E, which resulted in two values (i.e., within and across-hemisphere connectivity) per session for each subject similar to (Vidaurre et al., 2020).

Since changes in SNR of oscillations in the frequency band of interest lead to spurious changes in PS due to either more or less accurate phase estimation (Muthukumaraswamy and Singh, 2011), we applied a correction for SNR in the statistical analyses.

2.13. Multiverse Analysis

Overall, in the current multiverse analysis, we considered 24 pipelines based on all possible combinations of methods for the aforementioned processing steps (Fig. 2A). By selecting these pipelines, we aimed to assess the effects of data-independent (eLORETA, AVG-F, BB, anatomical ROIs) and task- or subject-dependent (LCMV, SVD, NB, task-based ROIs) methods on the estimated values of SNR and connectivity, their relationship with BCI performance, and changes over time. For each pipeline, we estimated the values of SNR as well as within- and across-hemisphere PS. Then, we tested their relationship with performance and changes over time, as described below.

2.14. Statistical Analysis

Statistical analysis was performed in R 4.2.2 (R Core Team, 2022). We used one-sample t-tests to analyze differences in mu power between trials corresponding to the imaginary movements. Also, we used Welch's two-sample t-test to check for group differences in performance and SNR. To assess the between-subject effects of SNR or phase synchronization on BCI performance, we correlated accuracy and a predictor variable (SNR or PS) after averaging them over all sessions for each subject. Within-subject effects of SNR and PS on accuracy as well as changes in SNR and PS over time were assessed with linear mixed-effect (LME) models using lme4 (Bates et al., 2015) and lmerTest (Kuznetsova et al., 2017) packages. The values of continuous variables were normalized before fitting the LMEs by subtracting the mean and dividing over the standard deviation. The denominator degrees of freedom in the LMEs were adjusted according to Satterthwaite's method (Satterthwaite, 1946). P-values less than 0.05 were considered significant. The LME models that correspond to the research questions (relationship between SNR or PS and BCI performance, changes in SNR and PS over time, and effects of different processing methods on SNR and PS) are presented in Table 1. Additionally, we used linear mixed models to investigate the relationship between SNR and PS values.

Effect	**Model**	
Relationship between SNR and Phase Synchronization (PS) Values		
SNR $\rightarrow$ PS	PS $\sim$ 1 + SNR + (1 | Subject)	(*)
Relationship between SNR or PS and BCI Performance (Accuracy)		
SNR $\rightarrow$ Acc.	Accuracy $\sim$ 1 + SNR + (SNR | Subject)	(*)
PS $\rightarrow$ Acc.	Accuracy $\sim$ 1 + PS + (1 | Subject)	(*)
PS $\rightarrow$ Acc. | SNR	Accuracy $\sim$ 1 + SNR + PS + (1 | Subject)	(*)
Longitudinal Changes in Accuracy, SNR, and Phase Synchronization		
Session $\rightarrow$ Acc.	Accuracy $\sim$ 1 + Session + (Session | Subject)	
Session $\rightarrow$ SNR	SNR $\sim$ 1 + Session + (Session | Subject)	(*)
Session $\rightarrow$ PS	PS $\sim$ 1 + Session + (1 | Subject)	(*)
Session $\rightarrow$ PS | SNR	PS $\sim$ 1 + SNR + Session + (1 | Subject)	(*)
Effects of the Processing Methods on the Estimated SNR and Phase Synchronization		
Methods $\rightarrow$ SNR	SNR $\sim$ Inv. + ROI + Mask + (1 | Subject) + (1 | Pipeline)	
Methods $\rightarrow$ PS	PS $\sim$ Inv. + ROI + Band + Mask + (1 | Subject) + (1 | Pipeline)	
Methods $\rightarrow$ PS | SNR	PS $\sim$ SNR + Inv. + ROI + Band + Mask + (1 | Subject) + (1 | Pipeline)	

(*) random effect of the processing pipeline (1 | Pipeline) was added in the joint multiverse analysis.

Table 1: Linear mixed-effects models that were used for the assessment of the effects of interest. Notation X $\rightarrow$ Y | Z corresponds to the effects of X on Y, controlled for Z. Acc., ROI, and Inv. stand for Accuracy, Extraction of ROI Time Series and Inverse Modeling, respectively. Random slopes were added to the models as long as they converged for all of the considered pipelines.

For the multiverse analysis, we have considered two approaches: split and joint analysis. In the split analysis, we fitted a separate mixed model for each of the pipelines and then aggregated

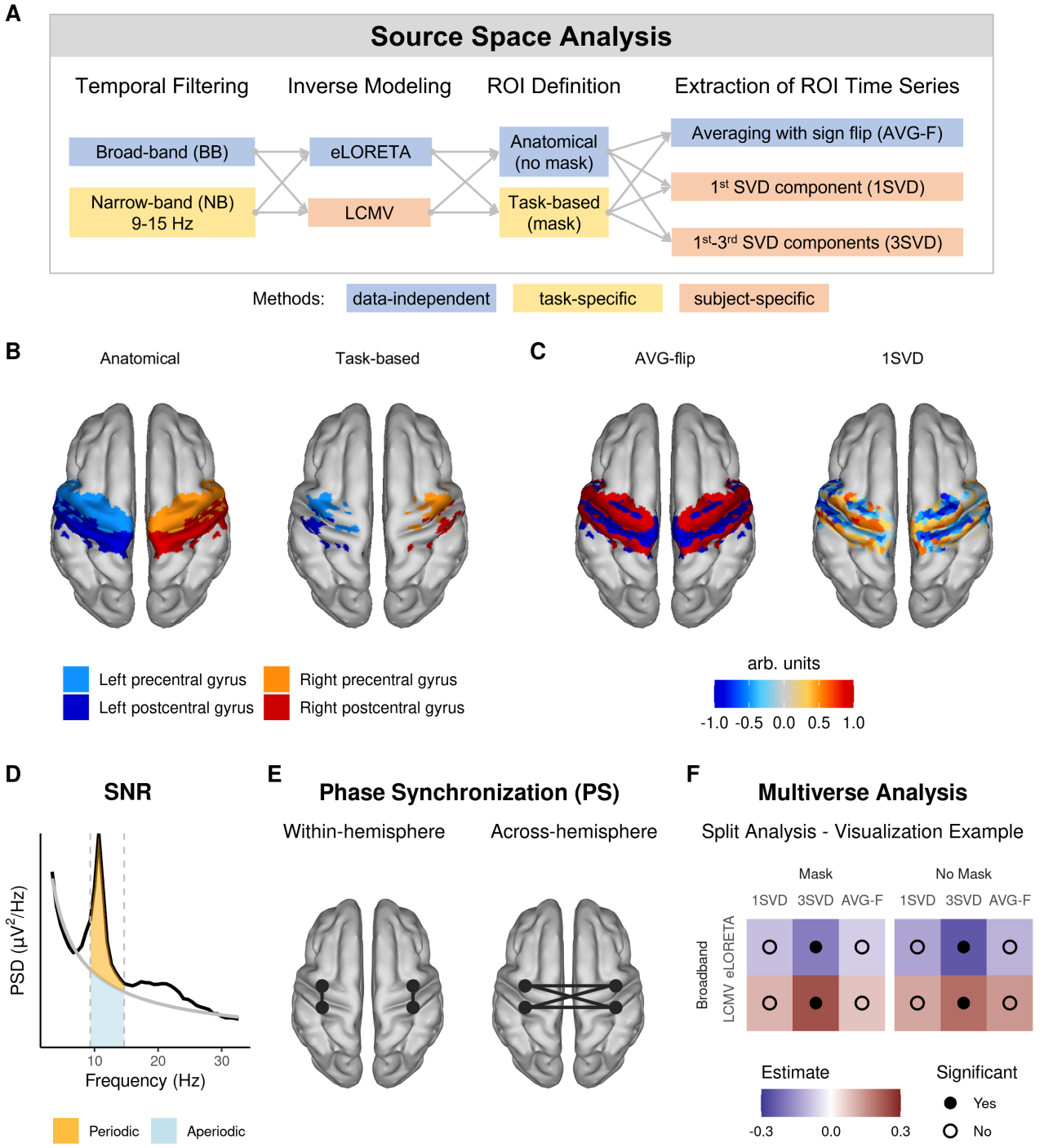

Figure 2: Overview of the multiverse analysis of SNR and phase synchronization in the source space. (A) 24 combinations of the data-independent and task- or subject-specific methods were used in the current analysis. (B) Anatomical (No Mask) and task-based (Mask, derived using CSP) definitions of sensorimotor ROIs. (C) AVG-F and 1SVD weights for all sources within sensorimotor ROIs for an exemplary subject. (D) SNR was estimated as the ratio of the total (periodic + aperiodic) power and the power of the aperiodic component in the 9-15 Hz frequency range. The gray line depicts the 1/f fit obtained with FOOOF. (E) Phase synchronization values were averaged over the within-hemisphere and across-hemisphere interactions between sensorimotor ROIs. (F) Statistical results were aggregated in a table to assess the robustness of effects to the selection of the pipeline. Estimated correlations (between-subject effect) or beta weights (within-subject effect) were coded with color, and the significance of the effects was indicated by filled black dots.

the results in the form of a table as shown in Fig. 2F. With this representation, one can visually inspect whether the effect is robust or specific to one of the processing steps.

In the joint analysis, we first combined the data from all pipelines and then ran the statistical analysis while including the pipeline as a random factor in the linear mixed model (see the asterisks in the rows of Table 1). This way, we obtained one result for each research question based on the combined evidence from all the considered pipelines. Additionally, we calculated the consistency between pipelines as the number of pipelines that led to the same result as the joint analysis. Finally, we analyzed the effects of different processing methods on the estimated values of SNR and phase synchronization.

For all of the research questions, we applied the Bonferroni correction for multiple comparisons ($m = 6$) since we considered two options (within- and across-hemisphere) for three PS measures (ImCoh, LagCoh, and coherence). We did not apply correction for multiple comparisons due to having 24 pipelines, since we assumed that each pipeline is equally likely to be selected for the estimation of PS. Instead, the split analysis was performed to investigate which of the individual pipelines led to a significant result.

3. Results

3.1. Performance improved over time and did not differ between groups

The average accuracy of BCI control increased from 64.3 % in the baseline session to 76.5 % in the last session (Fig. 1D). Changes over time were statistically significant ($\beta = 0.12$, $t(57.9) = 2.8, p = 0.006, 95\%$ CI: $[0.03, 0.20]$). As shown in the previous analyses of the same dataset (Stieger et al., 2020), there were no significant differences in the mean accuracy between MBSR (70.99 %) and control (71.08 %) groups: $t(57.5) = -0.02, p = 0.98$, Cohen's $d = -0.006, 95\%$ CI of the difference $[-0.07, 0.07]$ (Fig. 1E). The mean accuracy of all participants was 71.03%. At the same time, the intra-individual variability of performance was quite considerable (Fig. 1F). We used linear mixed models to account for this variability in the current analysis.

3.2. Sensorimotor ROIs contained the majority of task-relevant sources

For some of the source space analysis pipelines, we identified the task-relevant sources by fitting CSP to distinguish between imaginary movements of two hands. For this purpose, we used EEG during the target presentation interval as it showed a difference in mu power between the imaginary movements primarily over the sensorimotor areas (Fig. 1C). Resulting CSP patterns and the corresponding power spectra for left- and right-hand movements are shown in Fig. 3A and Fig. 3B, respectively. These patterns were source reconstructed with eLORETA to assess the contribution of individual sources to CSP components (Fig. 3C). Sources that exceeded the 97.5th percentile of activity strength were considered task-relevant, and table S1 shows that the sensorimotor ROIs contained the highest number of selected sources. Task-relevant sources formed the resulting source mask (Fig. 3D), which was applied to the anatomical definitions of sensorimotor ROIs to obtain a task-based reduced representation (Fig. 2B).

3.3. Laplace SNR was correlated with BCI performance but did not change over time

In the sensor space analysis, we used FOOOF to estimate average values of SNR at C3 and C4 after the Laplace transform. Examples of average power spectra for three representative subjects with different levels of Laplace SNR are shown in Fig. 4A. Similar to performance, Laplace SNR did not differ significantly between the participant groups as shown in Fig. 4B ($t(59.7) = 1.09, p = 0.28$, Cohen's $d = 0.28, 95\%$ CI of the difference: $[-0.63, 2.1]$). Group-average SNR for different sessions is shown in Fig. 4C.

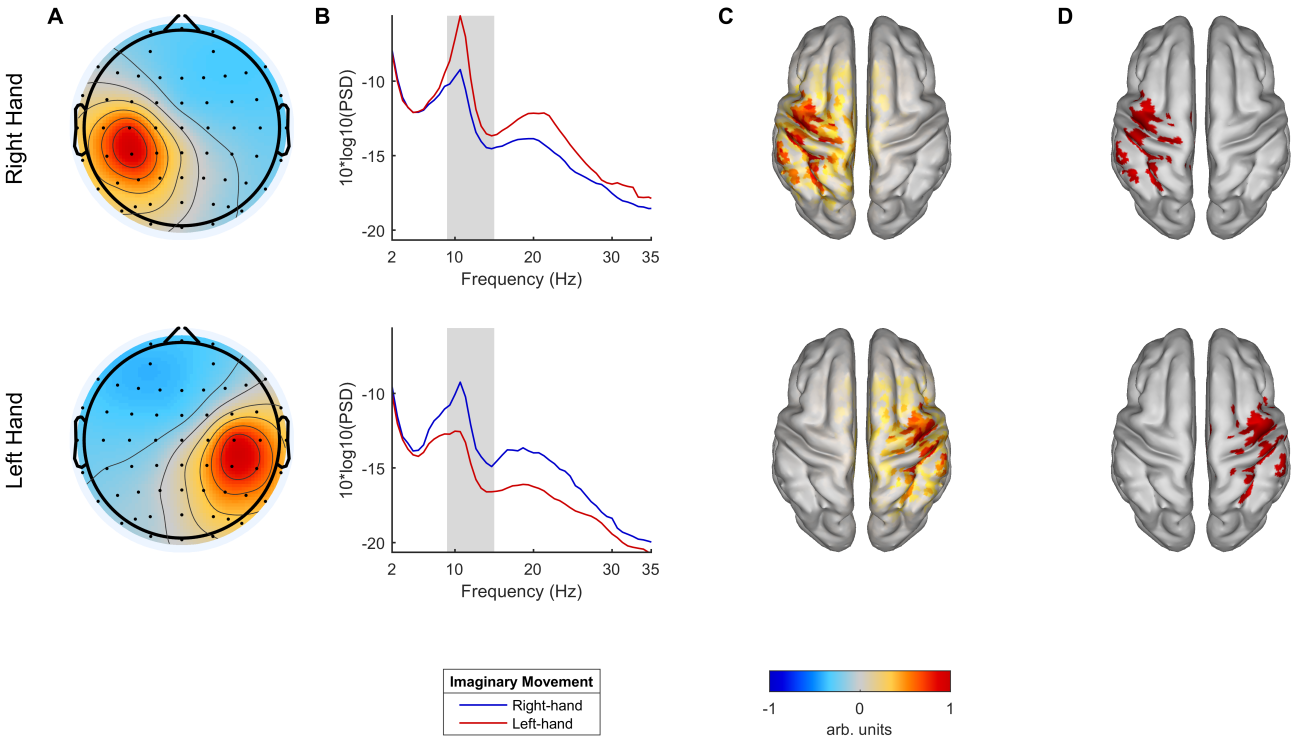

Figure 3: The task-relevant sources were identified through applying CSP to the EEG data during the target presentation interval after filtering in the 9-15 Hz frequency band. (A) Spatial patterns corresponding to the CSP filters that best discriminate imaginary movements of the right (upper row) and left (lower row) hands. Values were scaled to the [-1, 1] range. (B) Grand average power spectra of the CSP components corresponding to the spatial patterns from (A). The shaded area depicts the 9-15 Hz frequency band that was used to fit CSP. (C) Source reconstruction (absolute values, scaled to [-1, 1] range) of the spatial patterns from (A) with eLORETA. (D) Sources that exceeded the 97.5th percentile of activity strength were considered the most relevant for the execution of the motor imagery task.

Similar to (Blankertz et al., 2010a), we checked whether Laplace SNR was related to successful performance in the BCI training. Subject-average values of Laplace SNR were positively correlated with accuracy ($r = 0.35, t(60) = 2.9, p = 0.005, 95\%$ CI: $[0.11, 0.55]$), showing a between-subject effect of SNR on performance (Fig. 4D). Additionally, the within-subject effect of SNR on accuracy was significant, as assessed with a linear mixed model ($\beta = 0.29, t(57.2) = 5.22, p < 0.001, 95\%$ CI: $[0.18, 0.40]$). Figure 4E illustrates the observed within-subject effect.

Then, we investigated whether Laplace SNR changed over time due to the training, but longitudinal changes were not significant ($\beta = -0.03, t(51.2) = -1.11, p = 0.27, 95\%$ CI:$[-0.07, 0.02]$). Individual and group-level trends are shown in Fig. 4F.

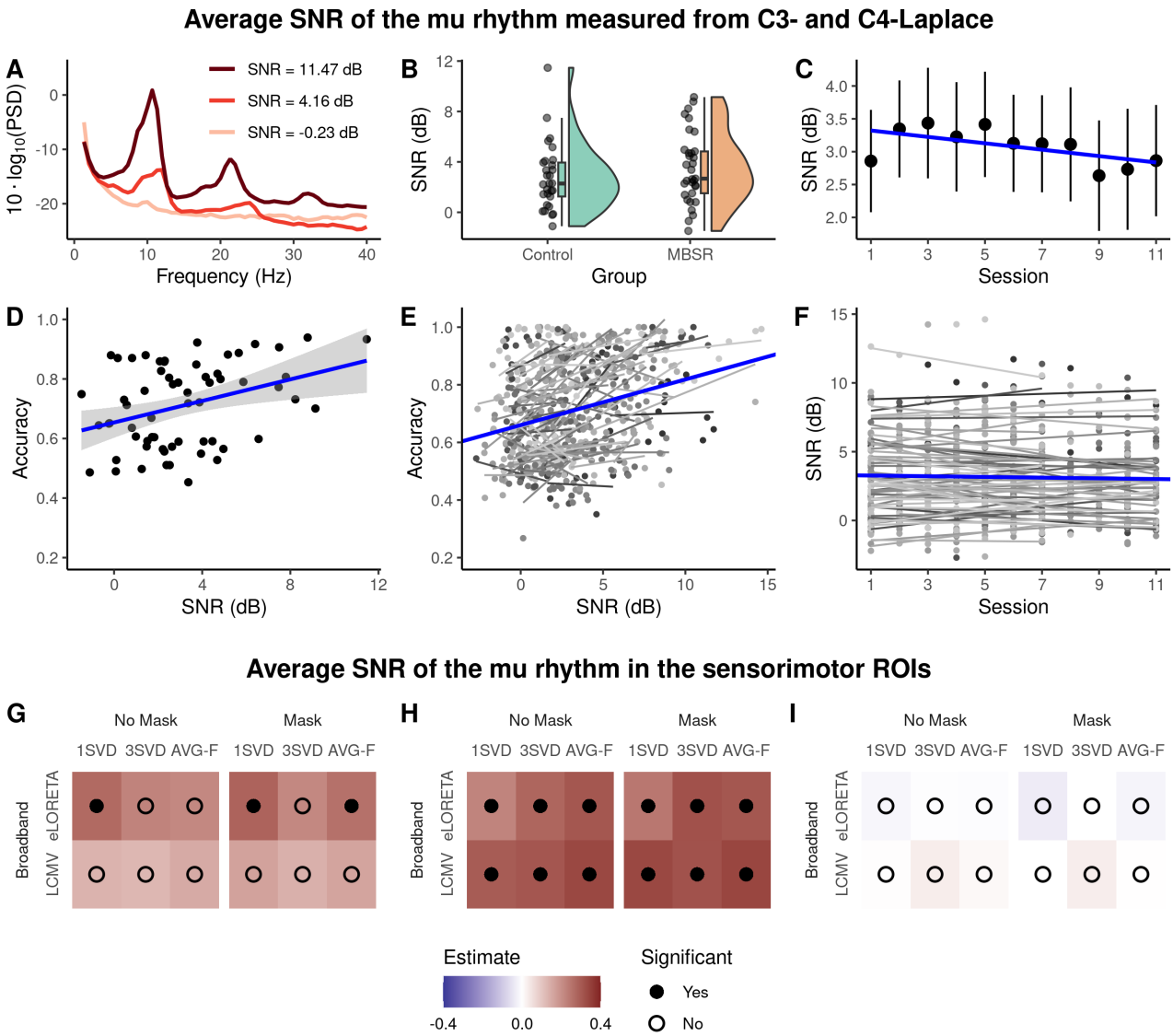

Figure 4: Laplace and ROI SNR showed both between- and within-subject effects on BCI performance and did not change systematically throughout the training. (A) Examples of resting-state power spectra (average of C3- and C4-Laplace over all sessions) for representative subjects with different levels of Laplace SNR. (B) The difference in SNR between groups was not significant. (C) Dynamics of group-average SNR across sessions. (D) Accuracy positively correlated with SNR after averaging over all sessions. Each point corresponds to a single participant. (E) Within-subject variability of BCI performance was related to session-to-session changes in SNR. Each point corresponds to a single session. Within-subject (gray) and group-level (blue) linear trends are shown. (F) No longitudinal changes were observed for SNR. Within-subject (gray) and group-level (blue) linear trends are shown. (G-I) Multiverse analysis similar to (D-F) but for ROI SNR in the source space showed high consistency of SNR-related effects across the data processing pipelines.

3.4. Effects of SNR, but not phase synchronization, were stable in the multiverse analysis

For the ROI SNR and phase synchronization, we applied a multiverse analysis to investigate the robustness of the observed effects to the selection of the pipeline. Figures 4G and 4H show that the estimated effects of ROI SNR on accuracy were positive for all 12 broad-band pipelines both on the between- and within-subject level, respectively. Additionally, on the within-subject level, all effects were significant. Figure 4I shows that no significant longitudinal changes in ROI SNR were observed for all considered pipelines. Overall, the results of the multiverse analysis for ROI SNR corresponded to the results for Laplace SNR and showed that the selection of the pipelines did not affect the observed effect of SNR on performance and changes in SNR.

For the phase synchronization, we first checked whether the grand-average spectra of within- and across-hemisphere values of PS measures show a pronounced peak in the mu frequency range. Such a peak indicates that the interaction is specific to the ongoing mu oscillations. As shown in Fig. 5A for a selection of pipelines, the peak was pronounced in most cases. However, within-hemisphere coherence estimated using the first SVD component showed almost identical values in the whole frequency range. In this case, it might occur due to the volume conduction, which equally affects all the frequencies.

In line with the previous studies (Bayraktaroglu et al., 2013; Vidaurre et al., 2020), we observed a robust positive effect of SNR on ImCoh and LagCoh, which are not sensitive to both spurious (caused by volume conduction) as well as genuine zero-lag interactions (Fig. 5B). In contrast, the effects of SNR on coherence were less consistent between pipelines and differed in sign depending on the selection of the processing methods. Overall, these results confirm that it is necessary to correct for SNR in the analyses of effects related to phase synchronization.

Then, we investigated the relationship between phase synchronization and accuracy as well as changes in PS over time. For both research questions, effects were not significant for the majority of the pipelines and PS measures (Fig. 6). Nevertheless, the pipelines that led to significant results often corresponded to a choice of a particular method at different processing steps. For example, the effects of within-hemisphere ImCoh and LagCoh on accuracy were more likely to be significant when inverse modeling was performed with an LCMV beamformer (Fig. 6A, rows 2, 4, and 6 from the top). In this case, pipeline-specific results showed up as stripes in the visualization. A different tendency was observed for the between-subject effect of phase synchronization on accuracy (Fig. S1) as well as longitudinal changes in PS (Fig. S2): When assessing phase synchronization using coherence, significant effects were more likely to emerge than for other PS measures. Overall, the effects of connectivity on performance were not significant for the majority of the pipelines, and the direction of the effects was not consistent between different pipelines and PS measures.

Finally, we ran a joint analysis for all research questions by pooling together the data from all of the pipelines and fitting one linear mixed model per question (Fig. 7). Once again, the aforementioned effects of SNR on accuracy and phase synchronization were significant and robust to the selection of the pipeline. Effects of ImCoh and LagCoh on accuracy were significant, but only before correction for SNR and less consistent between considered pipelines. Based on the evidence from all of the pipelines, across-hemisphere coherence significantly increased over the course of the training. Statistical results are presented in Table S2.

3.5. The selection of processing methods affected the estimated values of SNR and PS

Effects of processing methods on the estimated values of SNR and PS were assessed with a linear mixed model. Processing steps were modeled as fixed effects, and we investigated whether the selection of the pipeline systematically affected the estimated values of SNR and PS. Table 2 contains the estimated t-values for all predictors, and significant effects are highlighted in bold. Stars indicate that the effects remained significant after the correction for multiple comparisons.

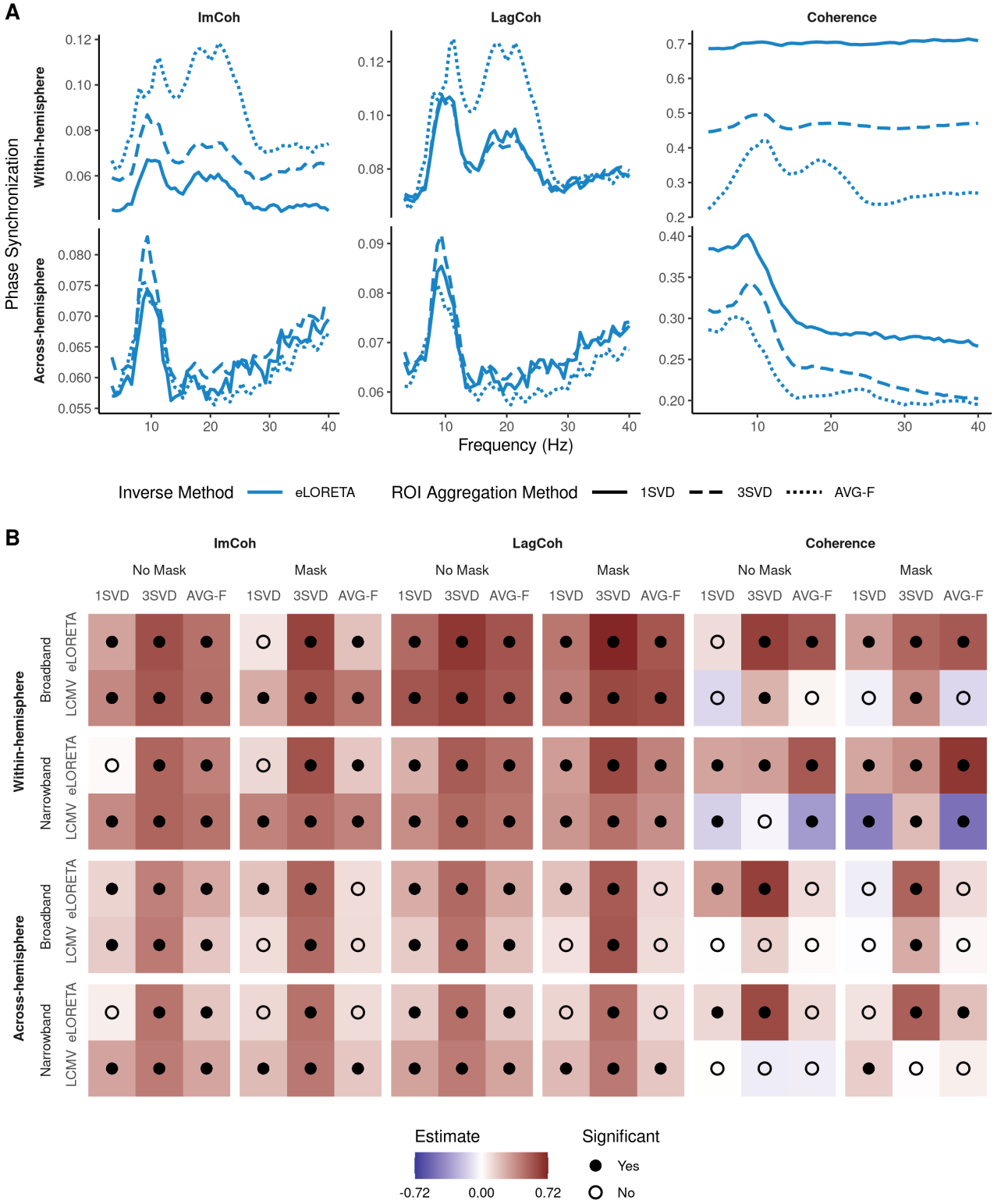

Figure 5: Multiverse analysis of the relationship between SNR and phase synchronization measures. (A) Grand average spectra of within- (top row) and across-hemisphere (bottom row) values of ImCoh, LagCoh, and coherence (columns: left to right) for the broadband pipelines with eLORETA, anatomical definitions of ROIs, and different ROI aggregation methods. (B) SNR showed consistent positive effects on ImCoh and LagCoh but not on coherence, both for within- and across-hemisphere phase synchronization.

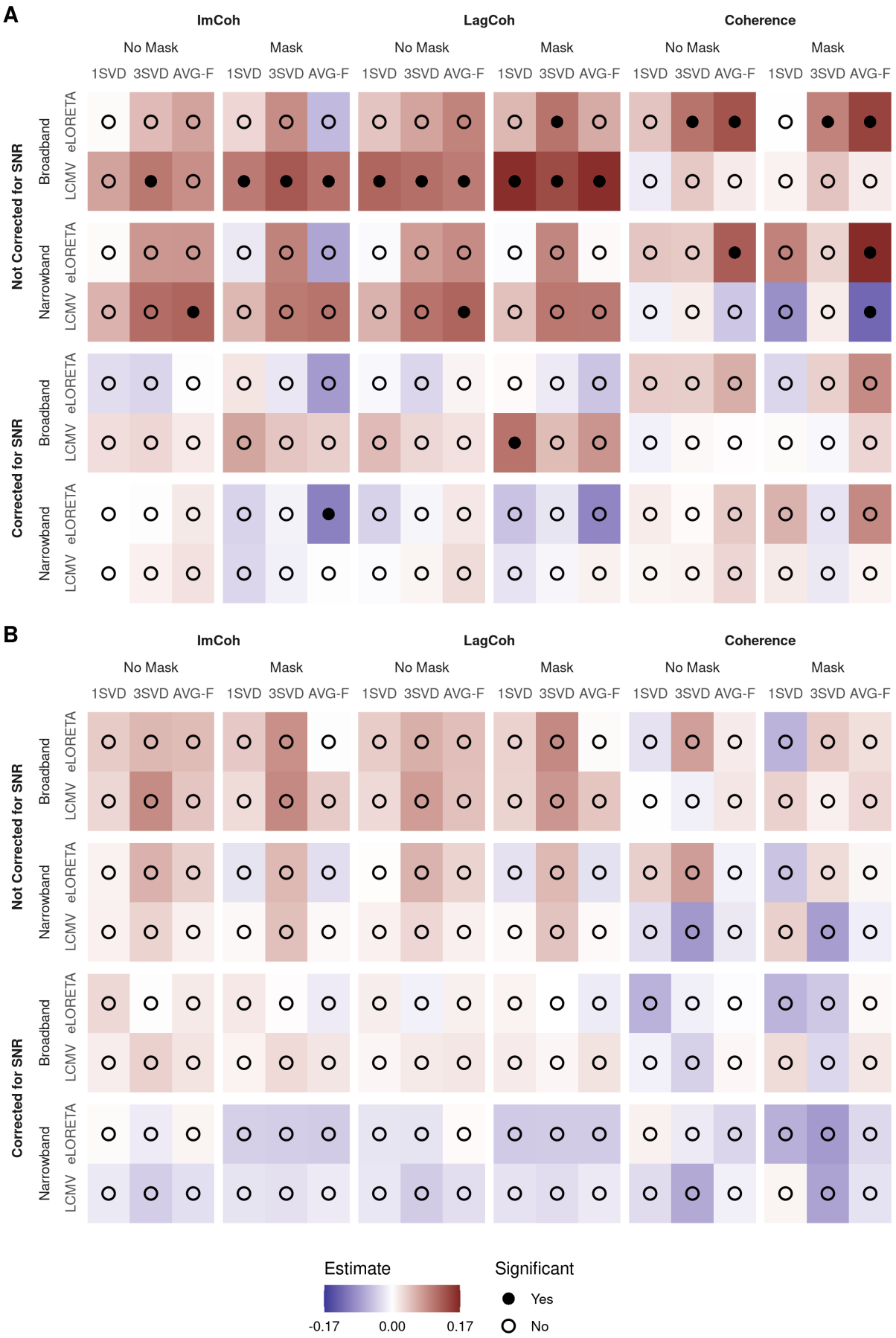

Figure 6: Within-subject effects of phase synchronization on BCI performance in the split multiverse analysis. Bonferroni correction for multiple ($m = 6$) comparisons was applied. Panels (A) and (B) correspond to within- and across-hemisphere phase synchronization, respectively.

Figure 7: Overview of the observed within-subject effects in the joint multiverse analysis. Bonferroni correction for multiple ($m = 6$) comparisons was applied to account for several phase synchronization measures. Color codes the number of pipelines that led to the same statistical result as the joint analysis.

First, we observed that the values of SNR were higher when LCMV was used for inverse modeling as compared to eLORETA (Fig. 8A), while other processing steps did not have a significant effect on SNR. We investigated the increase in SNR in more detail since the quality of the source reconstruction with LCMV depends on the SNR (Van Veen et al., 1997), and SNR played an important role in the previous analyses. For this purpose, we compared values of SNR within pairs of pipelines, which differed only in the method for inverse modeling. As shown in Fig. S3, the difference in the estimated SNR between the pipelines that include LCMV and eLORETA was positive and most pronounced for low values of SNR. For higher values for SNR, the difference either vanished or became negative.

PS measures were affected by the selection of methods for all processing steps. When the 3SVD method was used for the extraction of ROI time series as compared to 1SVD, coherence decreased (Fig. 8C,F), while ImCoh increased. Filtering in a narrow frequency band significantly decreased all PS measures apart from within-hemisphere coherence, and Fig. 8B and 8E illustrate this effect for within- and across-hemisphere ImCoh, respectively. Additionally, for within-hemisphere phase synchronization, AVG-F and anatomical definitions of ROIs led to an increase in ImCoh and LagCoh as well as a decrease in coherence compared to 1SVD and task-based definitions of ROIs, respectively. Finally, LCMV led to smaller values of ImCoh and LagCoh than eLORETA (Fig. 8D).

4. Discussion

In the current study, we investigated the role of SNR and phase synchronization of the mu rhythm in sensorimotor brain areas as predictors of BCI performance in a multi-session training using a publicly available dataset (Stieger et al., 2021). The dataset contained EEG recordings

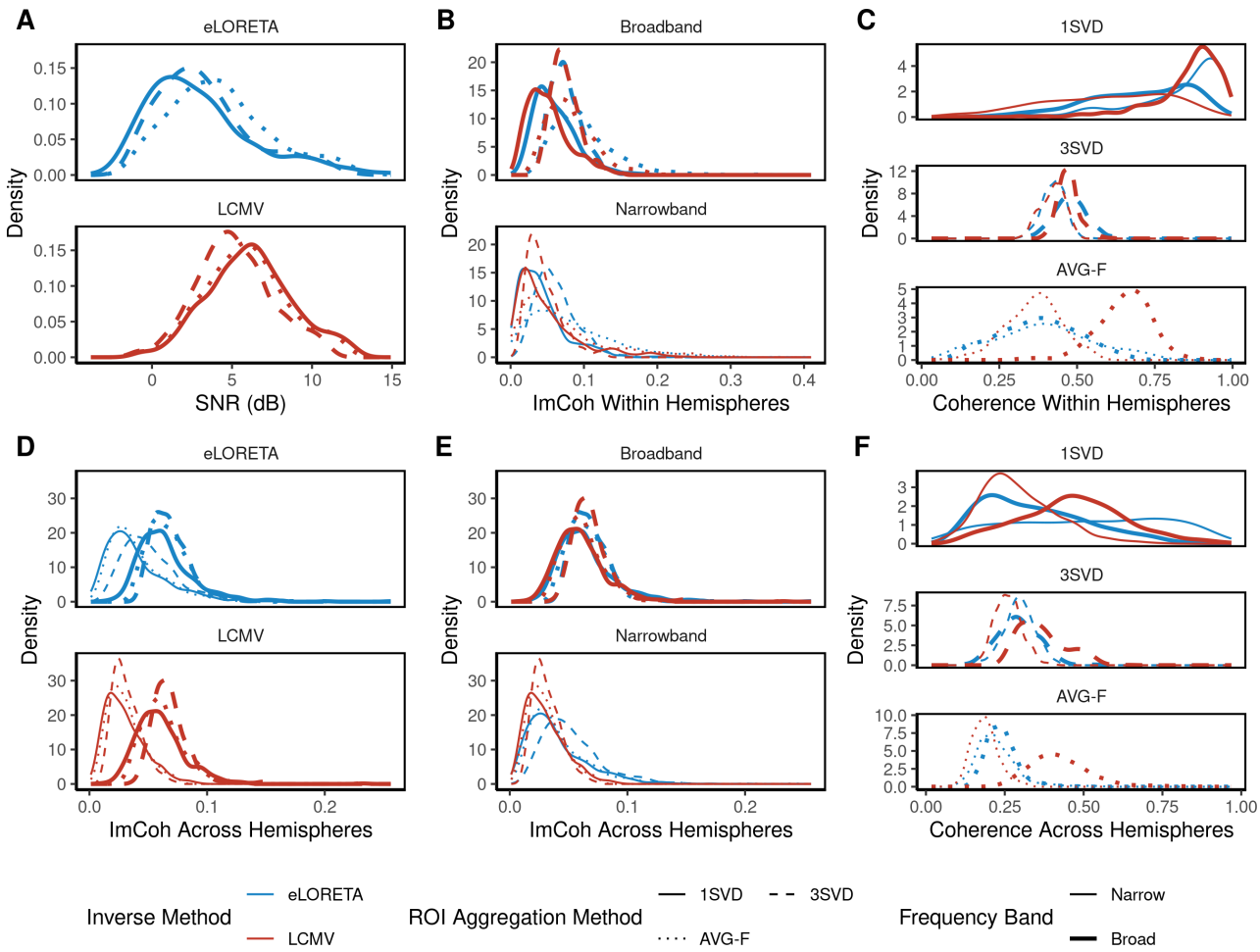

Figure 8: Selection of the processing methods affected estimated values of SNR and phase synchronization as indicated by shifts in the empirical probability density functions. Only pipelines with anatomical definitions of ROIs (No Mask) are displayed. (A) SNR was higher when LCMV was used as compared to eLORETA. (B) Filtering in a narrow frequency band led to smaller values of ImCoh within hemispheres. (C) Method for extraction of ROI time series affected values of within-hemisphere coherence. (D) LCMV led to smaller values of across-hemisphere ImCoh compared to eLORETA. (E) Same as B, but for ImCoh across hemispheres. (F) Same as C, but for across-hemisphere coherence.

Value	Inverse Method LCMV | eLORETA	ROI Method 3SVD | 1SVD	ROI Method AVG-F | 1SVD	Source Mask With | Without	Band NB | BB
SNR	**8.01***	-1.85	1.1	1.29	—
WH ImCoh	-1.9	**3.31***	**2.48**	**-4.16***	**-2.15**
WH LagCoh	**-3.55***	-1.51	**2.16**	-1.53	**-7.5***
WH Coherence	0.42	**-5.55***	-2.07	**3.71***	-1.18
AH ImCoh	**-4.91***	**3.28***	-0.13	-0.64	**-17.33***
AH LagCoh	**-3.24***	1.69	-1.02	-1.33	**-13.46***
AH Coherence	0.96	-1.42	**-2.21**	-1.83	**-2.5**
WH ImCoh | SNR	**-2.83**	**3.54***	**2.37**	**-4.33***	**-2.16**
WH LagCoh | SNR	**-6.95***	-0.65	1.61	-2.05	**-7.27***
WH Coherence | SNR	0.14	**-5.47***	**-2.11**	**3.66***	-1.17
AH ImCoh | SNR	**-6.81***	**3.74***	-0.4	-0.95	**-17.42***
AH LagCoh | SNR	**-4.92***	2.06	-1.25	-1.59	**-13.17***
AH Coherence | SNR	0.53	-1.31	**-2.25**	-1.88	**-2.48**

Table 2: Summary of the observed effects (t-values) of different processing methods on the estimated values of SNR and phase synchronization. Significant effects are highlighted in bold, and stars indicate that the effects remained significant after Bonferroni correction for multiple ($m = 6$) comparisons. Columns correspond to different processing steps, and a positive t-value for $Y|X$ denotes that SNR or PS was higher when Y was used compared to X. X | SNR denotes that a correction for SNR was applied. WH and AH stand for within- and across-hemisphere, respectively.

from a multi-session BCI training based on a cursor control paradigm. The performance of the participants was assessed with the accuracy of completed trials and improved significantly for some but not all participants throughout the training. Overall, the mean accuracy was comparable to other BCI studies and similar to the 70% threshold, which is commonly used to identify good performers (e.g., in Sannelli et al. (2019) and Leeuwis et al. (2021)). While the increase in group-average performance was not prominent between sessions 2 and 10, a considerable level of intra-individual variability of performance was observed. We used linear mixed models to account for this variability and investigate the relationship between SNR, PS, and BCI performance, as well as longitudinal changes in SNR and PS due to training. We performed the analysis in sensor space using the Laplacian transform and in source space, combining several processing pipelines in a multiverse analysis. In the following, we discuss the results of the study and their prospective applications.

4.1. SNR in the context of sensorimotor BCI training

Previous studies have shown that the signal-to-noise ratio of the mu rhythm estimated at C3 and C4 channels after the Laplacian transform correlated with the accuracy of BCI control (Blankertz et al., 2010a; Acqualagna et al., 2016; Sannelli et al., 2019). We also observed a positive correlation between Laplace SNR and accuracy after averaging over all sessions, which reflects a between-subject effect of SNR on performance. Additionally, we observed a within-subject effect of Laplace SNR on accuracy. That is, not only do participants with a higher SNR of the mu rhythm tend to perform better, but the same participant tends to perform better on the days when SNR is higher as well.

In general, larger SNR is associated with stronger lateralization of the mu rhythm during imaginary movements, leading to a higher classification or control accuracy (Maeder et al., 2012). Our results show that this finding, previously observed primarily for the single experimental sessions, generalizes to longitudinal settings and has two important consequences. First, changes in overall performance should be controlled for the changes in SNR to make conclusions about other possible neurophysiological factors. Second, experimental adjustments leading to

an increase in SNR might also translate to a performance improvement. It is important to note that SNR might affect BCI performance at least in two different ways. On the one hand, participants with low SNR of the mu rhythm might not be able to perform vivid imaginary movements and modulate their brain activity strongly enough. In this case, "quasi-movements" (i.e., real movements minimized to such an extent that they cannot be detected by objective measures) could be used to train participants to perform the motor imagery better (Nikulin et al., 2008). On the other hand, high SNR of the mu rhythm might translate into a more reliable feedback signal, which would in turn allow participants to train the imaginary movements more efficiently. If this is the case, training for participants with low SNR of the mu rhythm could be based on other features of brain activity that might provide a higher SNR. For example, Tao et al. (2021) has shown that motor imagery led to a decrease in inter-trial phase coherence during steady-state stimulation of the median nerve. Moreover, there is still a considerable amount of unexplained variance in BCI performance, which could be attributed to other psychological (such as motivation or concentration) and lifestyle (sports or musical instrument training) factors. These factors remain a subject of extensive research in the BCI community (Hammer et al., 2012; Jeunet et al., 2015) and could also be manipulated to improve BCI performance.

Furthermore, we investigated whether Laplace SNR itself could change throughout sensorimotor BCI training but observed no evidence of longitudinal changes. This result could be related to the structure of the cursor control tasks. Typically, post-effects of BCI or neurofeedback are observed when the whole training is based on a fixed direction of modulation of brain activity, for example, up-regulation of alpha power (Zoefel et al., 2011). In contrast, cursor control tasks in the analyzed dataset always contained trials with mutually opposite ways of modulation of the mu rhythm (left- versus right-hand imaginary movements or motor imagery versus relaxation). Therefore, on average, task-related modulation of the mu rhythm may not have a cumulative effect across many sessions. In addition, Popov et al. (2023) have also reported an excellent (ICC = 0.83) test-retest reliability of the periodic component of the alpha power in the sensorimotor regions. While this finding goes in line with the absence of longitudinal changes in SNR in the analyzed dataset, there still was a within-subject effect of SNR on BCI performance. This result could be explained if SNR is a trait feature that is affected by measurement-related effects (e.g., different placement of the electrodes) on different training days. Nevertheless, measurement-related effects could, in turn, make the detection of longitudinal changes in SNR harder.

In our study, both the positive effect of SNR on accuracy and the absence of longitudinal changes in SNR were robust to the selection of the processing steps in the multiverse analysis, as the results were the same for all of the considered pipelines. Taken together with all the existing evidence for the role of SNR in BCI training, this result might suggest that the effect of SNR on accuracy is strong enough to overcome the variability in the estimation of SNR across different pipelines.

4.2. Phase synchronization in the context of sensorimotor BCI training

The absence of longitudinal changes in SNR is critical for discussing changes in other measures that were shown to be correlated with SNR such as phase synchronization or long-range temporal correlations (Samek et al., 2016; Vidaurre et al., 2020). Since a decrease in SNR typically leads to the attenuation of the aforementioned measures, their changes (e.g., due to learning, arousal, etc.) should be controlled for the concurrent changes in SNR.

In the current study, we analyzed three linear PS measures to combine the interpretability of coherence (as it reflects the strength of interaction) and robustness to zero-lag interactions provided by ImCoh and LagCoh. The estimation of PS was performed in the source space, and

several processing pipelines were combined in a multiverse analysis to assess the variability of the PS values and associated statistical effects. For most pipelines, we observed a peak in the mu range of the PS spectra, which reflects an interaction that is specific to mu oscillations.

In line with several previous studies (Bayraktaroglu et al., 2013; Vidaurre et al., 2020), we observed a positive correlation between the values of SNR and phase synchronization. On the one hand, higher SNR improves phase estimation and may spuriously lead to higher values of PS (Muthukumaraswamy and Singh, 2011). On the other hand, a higher PS between two neuronal populations is likely to co-occur with a higher level of synchronization within the populations, which would be manifested in higher SNR values (Schneider et al., 2021). Most likely, both factors contribute to a positive correlation between SNR and PS values. This correlation was very robust to the selection of the pipeline for PS measures that are not sensitive to zero-lag spurious interactions due to volume conduction (ImCoh and LagCoh). Effects of SNR on coherence were less consistent, which could be related to the remaining spatial leakage (i.e., signal mixing), especially in the case of nearby regions within the same hemisphere. Overall, our findings confirm that it is necessary to control for changes in SNR when analyzing phase synchronization.

We observed a significant positive within-subject effect of within- and across-hemisphere ImCoh and LagCoh on BCI performance. It was significant in the joint analysis and for a few separate pipelines in the split analysis. While this finding goes in line with the results of (Vidaurre et al., 2020), we observed no evidence for a between-subject effect (Fig. S1), which could serve as a direct replication. Also, all of the effects were not significant after correction for SNR. While motor imagery leads to a modulation of amplitude (ERD/ERS), it might not necessarily require phase synchronization as strongly as other tasks involving precise bilateral coordination (Shih et al., 2021). Our results suggest that phase synchronization was not related to BCI performance in the analyzed dataset.

Despite not showing high consistency between pipelines, there was a significant increase in across-hemisphere coherence throughout the training. This result could speak in favor of the optimization of the interaction between motor areas due to the training. However, since ImCoh and LagCoh did not show the same effect, there is not enough evidence to conclude that this increase is driven by a genuine interaction.

Overall, the findings related to phase synchronization were not as robust to the selection of the pipeline as they were for SNR. Hence, along with the recommendation from Mahjoory et al. (2017), it is necessary to include at least several analysis pipelines to account for the between-pipeline variability of PS values.

4.3. Effects of the processing methods on the estimated values of SNR and PS

The multiverse analysis also allowed us to compare SNR and PS values that were obtained by applying different combinations of methods for source space analysis to the same data. Since there is no ground truth available for real data, this comparison does not allow us to determine which methods work better or worse (Feuerriegel and Bode, 2022). Nevertheless, below we describe several observations that could be validated in simulations and used in future studies.

Inverse Modeling. SNR was higher on average when LCMV was used for inverse modeling as compared to eLORETA. Since LCMV is a data-driven approach, it might better adapt to different subjects and sessions and thereby extract oscillatory activity with higher SNR than eLORETA. Surprisingly, the difference in SNR between pipelines with LCMV and eLORETA was especially prominent for low values of SNR. However, it is not clear whether the improvement in the SNR of the extracted signal is due to better extraction of activity from the investigated ROIs or the remaining spatial leakage from other ROIs. At the same time, LCMV

led to a decrease in ImCoh and LagCoh compared to eLORETA. Previous studies (Mahjoory et al., 2017; Pellegrini et al., 2023) also observed the impact of the inverse method on the estimated PS values. While the reasons behind this decrease in PS are not clear, it is important to note that the selection of the inverse method also played a role in the split multiverse analysis. In particular, the effects of within-hemisphere ImCoh and LagCoh on BCI performance were significant only for pipelines that included LCMV (Fig. 6A).

Extraction of ROI Time Series. ROI time series were obtained by aggregation of time series of individual sources within the ROI, and the selection of the aggregation method affected all PS measures. In particular, for the within-hemisphere case, the first SVD component seemed to capture the remaining effects of volume conduction to a great extent, as indicated by the lack of a peak in the spectra of coherence (Fig. 5A) and the values of coherence that are very close to 1 (Fig. 8C). In contrast, when three SVD components were used for the calculation of the connectivity, a peak in the spectra was present, and coherence was generally lower, while ImCoh had higher values. This result might be caused by the averaging of pairwise connectivity values between different SVD components, which is more likely to result in a non-zero phase lag. Still, by including more than one component per ROI in the analysis, one might ensure that a genuine interaction between ROIs is captured. This observation goes in line with the recommendation to consider 3-4 SVD components per ROI from (Pellegrini et al., 2023). Averaging with sign flip, in general, led to similar PS values as 1SVD but seemed to capture the remaining effects of volume conduction less, as reflected by lower coherence and higher ImCoh (the effects were not significant after correcting for multiple comparisons).

Filtering. Filtering in a narrow band led to a decrease in all considered PS measures, but the reasons behind that are not clear. While it should not be caused by different ways of calculating PS (via the Fourier transform or via the analytic signal), simulations might be required to understand this result in detail.

ROI Definition. We investigated whether reducing anatomical definitions of ROIs to a subset of task-relevant sources could make the estimated SNR and PS values even more task-specific. The definition of the ROI played a role only for the estimation of within-hemisphere PS, potentially by reducing the size of the ROI and variability in the reconstructed time series of individual sources. Thereby, the effects of volume conduction became pronounced even stronger (higher coherence and lower ImCoh).

Overall, the combination of LCMV and several SVD components (the pipeline that was also recommended in a recent study by Pellegrini et al. (2023)) seems to provide higher SNR and capture interactions that are specific to the frequency band of interest even for nearby ROIs within the same hemisphere. However, the effects of different processing steps might still depend on the location (within- or across-hemisphere in our case) and the size of the interacting ROIs (Mahjoory et al., 2017).

4.4. Limitations

The current analysis was limited to four sensorimotor ROIs and did not include the whole-brain connectivity patterns as, for example, in (Corsi et al., 2020). This selection was based on previous studies showing that motor imagery BCI primarily leads to activation of the sensorimotor areas that we analyzed (Nierhaus et al., 2021). These ROIs contained the highest amount of task-relevant sources in the analyzed dataset as well (Table S1), thereby additionally validating the selection. As described before, there are several open questions regarding the estimation of connectivity, correlation with behavior, correction for SNR, and interpretation of the results. Analyzing only selected ROIs made it feasible to address these challenges by considering several options for each question.

There also exist other methods that were not included in the multiverse analysis to ensure computational feasibility, e.g., dynamic imaging of coherent sources (DICS; Gross et al. (2001)) for inverse modeling or fidelity weighting (Korhonen et al., 2014) for aggregation of ROI time series. However, the amount of pipelines considered in the current analysis already provides additional insights compared to a single pipeline. Still, it is important to keep in mind that even if similar results are obtained with multiple pipelines, it does not directly imply the genuineness of these results.

The final limitation is related to the longitudinal analysis. While the group-level improvement in performance was significant, group-average accuracy was similar across most sessions, which might reflect little evidence of training effects. Nevertheless, we utilized the observed within-subject variability and employed linear mixed models to estimate the effects of interest.

4.5. Conclusions

Overall, we observed that SNR had an effect on BCI performance both on the between- and within-subject levels: Participants with higher SNR tended to perform better, and the same participant also tended to perform better on the days when SNR was higher. Therefore, interventions that are suitable for increasing SNR might lead to an improvement in performance. Additionally, multiverse analyses allowed us to analyze the robustness of the investigated effects to the selection of the pipeline. The results suggest that SNR was a primary factor of the observed performance variability (as it robustly predicted accuracy and covaried with connectivity), while connectivity effects became non-significant after controlling for SNR and were less consistent across different pipelines. We observed no evidence of longitudinal changes in SNR and only weak evidence of an increase in the strength of the interaction between hemispheres during the training. At the same time, values of SNR and phase synchronization were significantly affected by the selection of the pipeline for source space analysis. Therefore, it is necessary to include several pipelines in the analysis to assess how robust the observed effects are and how high the between-pipeline variability is. This paper can serve as a template for future multiverse analyses as it represents an end-to-end fully repeatable pipeline from raw data to publishable report, and all the underlying data and scripts are publicly available.

Data and Code Availability

EEG recordings are publicly available at `https://doi.org/10.6084/m9.figshare.13123148`, and a detailed description of the dataset is provided in (Stieger et al., 2021). Analysis scripts are available at `https://github.com/ctrltz/bci-brain-connectivity`. Preprocessing data that is necessary to reproduce the analysis (indices of bad trials, channels, and ICA components, ICA weights, excluded sessions, etc.) are available at `https://osf.io/tcvyd`.

CRediT Authorship Contribution Statement

Nikolai Kapralov: Conceptualization, Data curation, Formal analysis, Investigation, Methodology, Software, Visualization, Writing – original draft, Writing – review & editing. **Mina Jamshidi Idaji:** Validation (Code Review), Writing – review & editing. **Tilman Stephani:** Methodology, Validation (Code Review), Writing – review & editing. **Alina Studenova:** Validation (Code Review), Writing – review & editing. **Carmen Vidaurre:** Software, Writing – review & editing. **Tomas Ros:** Writing – review & editing. **Arno Villringer:** Funding acquisition, Writing – review & editing. **Vadim Nikulin:** Conceptualization, Investigation, Methodology, Project administration, Supervision, Writing – Original Draft, Writing – review & editing.

Acknowledgements

We would like to thank the authors of the dataset for making it publicly available and James Stieger in particular for providing additional information about the dataset on request.

References

Abiri, R., Borhani, S., Sellers, E.W., Jiang, Y., Zhao, X., 2019. A comprehensive review of EEG-based brain-computer interface paradigms. J Neural Eng 16, 011001. doi:10.1088/1741-2552/aaf12e.

Acqualagna, L., Botrel, L., Vidaurre, C., Kübler, A., Blankertz, B., 2016. Large-scale assessment of a fully automatic co-adaptive motor imagery-based brain computer interface. PloS one 11, e0148886. doi:10.1371/journal.pone.0148886.

Ahn, M., Cho, H., Ahn, S., Jun, S.C., 2013. High theta and low alpha powers may be indicative of BCI-illiteracy in motor imagery. PLoS One 8, e80886. doi:10.1371/journal.pone.0080886.

Allison, B.Z., Neuper, C., 2010. Could anyone use a BCI?, in: Tan, D.S., Nijholt, A. (Eds.), Brain-Computer Interfaces: Applying our Minds to Human-Computer Interaction. Springer London, London, pp. 35–54. doi:10.1007/978-1-84996-272-8_3.

Babiloni, F., Cincotti, F., Babiloni, C., Carducci, F., Mattia, D., Astolfi, L., Basilisco, A., Rossini, P.M., Ding, L., Ni, Y., Cheng, J., Christine, K., Sweeney, J., He, B., 2005. Estimation of the cortical functional connectivity with the multimodal integration of high-resolution EEG and fMRI data by directed transfer function. Neuroimage 24, 118–131. doi:10.1016/j.neuroimage.2004.09.036.

Barnett, L., Seth, A.K., 2014. The MVGC multivariate Granger causality toolbox: a new approach to Granger-causal inference. J Neurosci Methods 223, 50–68. doi:10.1016/j.jneumeth.2013.10.018.

Bastos, A.M., Schoffelen, J.M., 2015. A Tutorial Review of Functional Connectivity Analysis Methods and Their Interpretational Pitfalls. Front Syst Neurosci 9, 175. doi:10.3389/fnsys.2015.00175.

Bates, D., Mächler, M., Bolker, B., Walker, S., 2015. Fitting linear mixed-effects models using lme4. Journal of Statistical Software 67, 1–48. doi:10.18637/jss.v067.i01.

Bayraktaroglu, Z., von Carlowitz-Ghori, K., Curio, G., Nikulin, V.V., 2013. It is not all about phase: amplitude dynamics in corticomuscular interactions. Neuroimage 64, 496–504. doi:10.1016/j.neuroimage.2012.08.069.

Blankertz, B., Acqualagna, L., Dähne, S., Haufe, S., Schultze-Kraft, M., Sturm, I., Ušćumlic, M., Wenzel, M.A., Curio, G., Müller, K.R., 2016. The Berlin Brain-Computer Interface: Progress Beyond Communication and Control. Front Neurosci 10, 530. doi:10.3389/fnins.2016.00530.

Blankertz, B., Sannelli, C., Halder, S., Hammer, E.M., Kübler, A., Müller, K.R., Curio, G., Dickhaus, T., 2010a. Neurophysiological predictor of SMR-based BCI performance. NeuroImage 51, 1303–1309. doi:10.1016/j.neuroimage.2010.03.022.

Blankertz, B., Tangermann, M., Vidaurre, C., Fazli, S., Sannelli, C., Haufe, S., Maeder, C., Ramsey, L., Sturm, I., Curio, G., Müller, K.R., 2010b. The Berlin Brain-Computer Interface: Non-Medical Uses of BCI Technology. Front Neurosci 4, 198. doi:10.3389/fnins.2010.00198.

Cervera, M.A., Soekadar, S.R., Ushiba, J., Millán, J.D.R., Liu, M., Birbaumer, N., Garipelli, G., 2018. Brain-computer interfaces for post-stroke motor rehabilitation: a meta-analysis. Ann Clin Transl Neurol 5, 651–663. doi:10.1002/acn3.544.

Chaudhary, U., Birbaumer, N., Ramos-Murguialday, A., 2016. Brain-computer interfaces for communication and rehabilitation. Nat Rev Neurol 12, 513–525. doi:10.1038/nrneurol.2016.113.

Corsi, M.C., Chavez, M., Schwartz, D., George, N., Hugueville, L., Kahn, A.E., Dupont, S., Bassett, D.S., De Vico Fallani, F., 2020. Functional disconnection of associative cortical areas predicts performance during BCI training. Neuroimage 209, 116500. doi:10.1016/j.neuroimage.2019.116500.

Delorme, A., Makeig, S., 2004. EEGLAB: an open source toolbox for analysis of single-trial EEG dynamics including independent component analysis. J Neurosci Methods 134, 9–21. doi:10.1016/j.jneumeth.2003.10.009.

Desikan, R.S., Ségonne, F., Fischl, B., Quinn, B.T., Dickerson, B.C., Blacker, D., Buckner, R.L., Dale, A.M., Maguire, R.P., Hyman, B.T., Albert, M.S., Killiany, R.J., 2006. An automated labeling system for subdividing the human cerebral cortex on MRI scans into gyral based regions of interest. Neuroimage 31, 968–980. doi:10.1016/j.neuroimage.2006.01.021.

Donoghue, T., Haller, M., Peterson, E.J., Varma, P., Sebastian, P., Gao, R., Noto, T., Lara, A.H., Wallis, J.D., Knight, R.T., Shestyuk, A., Voytek, B., 2020. Parameterizing neural power spectra into periodic and aperiodic components. Nat Neurosci 23, 1655–1665. doi:10.1038/s41593-020-00744-x.

Engel, A.K., Fries, P., Singer, W., 2001. Dynamic predictions: oscillations and synchrony in top-down processing. Nat Rev Neurosci 2, 704–716. doi:10.1038/35094565.

Engel, A.K., Gerloff, C., Hilgetag, C.C., Nolte, G., 2013. Intrinsic coupling modes: multiscale interactions in ongoing brain activity. Neuron 80, 867–886. doi:10.1016/j.neuron.2013.09.038.

Feuerriegel, D., Bode, S., 2022. Bring a map when exploring the ERP data processing multiverse: A commentary on Clayson et al. 2021. Neuroimage 259, 119443. doi:10.1016/j.neuroimage.2022.119443.

Fonov, V., Evans, A., McKinstry, R., Almli, C., Collins, D., 2009. Unbiased nonlinear average age-appropriate brain templates from birth to adulthood. NeuroImage 47, S102. doi:https://doi.org/10.1016/S1053-8119(09)70884-5.

Fonov, V., Evans, A.C., Botteron, K., Almli, C.R., McKinstry, R.C., Collins, D.L., Ball, W.S., Byars, A.W., Schapiro, M., Bommer, W., Carr, A., German, A., Dunn, S., Rivkin, M.J., Waber, D., Mulkern, R., Vajapeyam, S., Chiverton, A., Davis, P., Koo, J., Marmor, J., Mrakotsky, C., Robertson, R., McAnulty, G., Brandt, M.E., Fletcher, J.M., Kramer, L.A., Yang, G., McCormack, C., Hebert, K.M., Volero, H., Botteron, K., McKinstry, R.C., Warren, W., Nishino, T., Almli, C.R., Todd, R., Constantino, J., McCracken, J.T., Levitt, J., Alger, J., O'Neil, J., Toga, A., Asarnow, R., Fadale, D., Heinichen, L., Ireland, C., Wang, D.J., Moss,

E., Zimmerman, R.A., Bintliff, B., Bradford, R., Newman, J., Evans, A.C., Arnaoutelis, R., Pike, G.B., Collins, D.L., Leonard, G., Paus, T., Zijdenbos, A., Das, S., Fonov, V., Fu, L., Harlap, J., Leppert, I., Milovan, D., Vins, D., Zeffiro, T., Van Meter, J., Lange, N., Froimowitz, M.P., Botteron, K., Almli, C.R., Rainey, C., Henderson, S., Nishino, T., Warren, W., Edwards, J.L., Dubois, D., Smith, K., Singer, T., Wilber, A.A., Pierpaoli, C., Basser, P.J., Chang, L.C., Koay, C.G., Walker, L., Freund, L., Rumsey, J., Baskir, L., Stanford, L., Sirocco, K., Gwinn-Hardy, K., Spinella, G., McCracken, J.T., Alger, J.R., Levitt, J., O'Neill, J., 2011. Unbiased average age-appropriate atlases for pediatric studies. Neuroimage 54, 313–327. doi:10.1016/j.neuroimage.2010.07.033.

Frazier, J.A., Chiu, S., Breeze, J.L., Makris, N., Lange, N., Kennedy, D.N., Herbert, M.R., Bent, E.K., Koneru, V.K., Dieterich, M.E., Hodge, S.M., Rauch, S.L., Grant, P.E., Cohen, B.M., Seidman, L.J., Caviness, V.S., Biederman, J., 2005. Structural brain magnetic resonance imaging of limbic and thalamic volumes in pediatric bipolar disorder. Am J Psychiatry 162, 1256–1265. doi:10.1176/appi.ajp.162.7.1256.

Fries, P., 2005. A mechanism for cognitive dynamics: neuronal communication through neuronal coherence. Trends Cogn Sci 9, 474–480. doi:10.1016/j.tics.2005.08.011.

Goldstein, J.M., Seidman, L.J., Makris, N., Ahern, T., O'Brien, L.M., Caviness, V.S., Kennedy, D.N., Faraone, S.V., Tsuang, M.T., 2007. Hypothalamic abnormalities in schizophrenia: sex effects and genetic vulnerability. Biol Psychiatry 61, 935–945. doi:10.1016/j.biopsych.2006.06.027.

Gross, J., Kujala, J., Hamalainen, M., Timmermann, L., Schnitzler, A., Salmelin, R., 2001. Dynamic imaging of coherent sources: Studying neural interactions in the human brain. Proc Natl Acad Sci U S A 98, 694–699. doi:10.1073/pnas.98.2.694.

Halder, S., Agorastos, D., Veit, R., Hammer, E.M., Lee, S., Varkuti, B., Bogdan, M., Rosenstiel, W., Birbaumer, N., Kübler, A., 2011. Neural mechanisms of brain-computer interface control. Neuroimage 55, 1779–1790. doi:10.1016/j.neuroimage.2011.01.021.

Hammer, E.M., Halder, S., Blankertz, B., Sannelli, C., Dickhaus, T., Kleih, S., Müller, K.R., Kübler, A., 2012. Psychological predictors of SMR-BCI performance. Biol. Psychol. 89, 80–86. doi:10.1016/j.biopsycho.2011.09.006.

Hardwick, R.M., Caspers, S., Eickhoff, S.B., Swinnen, S.P., 2018. Neural correlates of action: Comparing meta-analyses of imagery, observation, and execution. Neurosci Biobehav Rev 94, 31–44. doi:10.1016/j.neubiorev.2018.08.003.

Haufe, S., Ewald, A., 2019. A Simulation Framework for Benchmarking EEG-Based Brain Connectivity Estimation Methodologies. Brain Topogr 32, 625–642. doi:10.1007/s10548-016-0498-y.

Huang, Y., Parra, L.C., Haufe, S., 2016. The New York Head—A precise standardized volume conductor model for EEG source localization and tES targeting. NeuroImage 140, 150–162. doi:10.1016/j.neuroimage.2015.12.019.

Hyvärinen, A., 1999. Fast and robust fixed-point algorithms for independent component analysis. IEEE Trans Neural Netw 10, 626–634. doi:10.1109/72.761722.

Jenkinson, M., Beckmann, C.F., Behrens, T.E., Woolrich, M.W., Smith, S.M., 2012. FSL. Neuroimage 62, 782–790. doi:10.1016/j.neuroimage.2011.09.015.

Jeunet, C., N'Kaoua, B., Subramanian, S., Hachet, M., Lotte, F., 2015. Predicting mental imagery-based BCI performance from personality, cognitive profile and neurophysiological patterns. PLOS ONE 10, 1–21. doi:10.1371/journal.pone.0143962.

Koles, Z.J., Lazar, M.S., Zhou, S.Z., 1990. Spatial patterns underlying population differences in the background EEG. Brain Topogr 2, 275–284. doi:10.1007/BF01129656.

Korhonen, O., Palva, S., Palva, J.M., 2014. Sparse weightings for collapsing inverse solutions to cortical parcellations optimize M/EEG source reconstruction accuracy. J Neurosci Methods 226, 147–160. doi:10.1016/j.jneumeth.2014.01.031.

Kruse, A., Suica, Z., Taeymans, J., Schuster-Amft, C., 2020. Effect of brain-computer interface training based on non-invasive electroencephalography using motor imagery on functional recovery after stroke - a systematic review and meta-analysis. BMC Neurol 20, 385. doi:10.1186/s12883-020-01960-5.

Kuznetsova, A., Brockhoff, P.B., Christensen, R.H.B., 2017. lmerTest package: Tests in linear mixed effects models. Journal of Statistical Software 82, 1–26. doi:10.18637/jss.v082.i13.

Lachaux, J.P., Rodriguez, E., Martinerie, J., Varela, F.J., 1999. Measuring phase synchrony in brain signals. Hum Brain Mapp 8, 194–208. doi:https://doi.org/10.1002/(SICI)1097-0193(1999)8:4<194::AID-HBM4>3.0.CO;2-C.

Lai, M., Demuru, M., Hillebrand, A., Fraschini, M., 2018. A comparison between scalp- and source-reconstructed EEG networks. Sci Rep 8, 12269. doi:10.1038/s41598-018-30869-w.

Leeb, R., Friedman, D., Müller-Putz, G.R., Scherer, R., Slater, M., Pfurtscheller, G., 2007. Self-paced (asynchronous) BCI control of a wheelchair in virtual environments: a case study with a tetraplegic. Comput Intell Neurosci 2007, 79642. doi:10.1155/2007/79642.

Leeuwis, N., Yoon, S., Alimardani, M., 2021. Functional Connectivity Analysis in Motor-Imagery Brain Computer Interfaces. Front Hum Neurosci 15, 732946. doi:10.3389/fnhum.2021.732946.

Maeder, C.L., Sannelli, C., Haufe, S., Blankertz, B., 2012. Pre-stimulus sensorimotor rhythms influence brain–computer interface classification performance. IEEE Transactions on Neural Systems and Rehabilitation Engineering 20, 653–662. doi:10.1109/TNSRE.2012.2205707.

Mahjoory, K., Nikulin, V.V., Botrel, L., Linkenkaer-Hansen, K., Fato, M.M., Haufe, S., 2017. Consistency of EEG source localization and connectivity estimates. NeuroImage 152, 590–601. doi:10.1016/j.neuroimage.2017.02.076.

Makris, N., Goldstein, J.M., Kennedy, D., Hodge, S.M., Caviness, V.S., Faraone, S.V., Tsuang, M.T., Seidman, L.J., 2006. Decreased volume of left and total anterior insular lobule in schizophrenia. Schizophr Res 83, 155–171. doi:10.1016/j.schres.2005.11.020.

Muthukumaraswamy, S.D., Singh, K.D., 2011. A cautionary note on the interpretation of phase-locking estimates with concurrent changes in power. Clin Neurophysiol 122, 2324–2325. doi:10.1016/j.clinph.2011.04.003.

Nierhaus, T., Vidaurre, C., Sannelli, C., Mueller, K.R., Villringer, A., 2021. Immediate brain plasticity after one hour of brain-computer interface (BCI). J Physiol 599, 2435–2451. doi:10.1113/JP278118.

Nikulin, V.V., Hohlefeld, F.U., Jacobs, A.M., Curio, G., 2008. Quasi-movements: a novel motor-cognitive phenomenon. Neuropsychologia 46, 727–742. doi:10.1016/j.neuropsychologia.2007.10.008.

Nolte, G., Bai, O., Wheaton, L., Mari, Z., Vorbach, S., Hallett, M., 2004. Identifying true brain interaction from EEG data using the imaginary part of coherency. Clin Neurophysiol 115, 2292–2307. doi:10.1016/j.clinph.2004.04.029.

Nolte, G., Galindo-Leon, E., Li, Z., Liu, X., Engel, A.K., 2020. Mathematical Relations Between Measures of Brain Connectivity Estimated From Electrophysiological Recordings for Gaussian Distributed Data. Front Neurosci 14, 577574. doi:10.3389/fnins.2020.577574.

Palva, S., Palva, J.M., 2007. New vistas for alpha-frequency band oscillations. Trends Neurosci 30, 150–158. doi:10.1016/j.tins.2007.02.001.

Pascual-Marqui, R.D., 2007. Discrete, 3D distributed, linear imaging methods of electric neuronal activity. Part 1: exact, zero error localization URL: https://arxiv.org/abs/0710.3341, doi:10.48550/ARXIV.0710.3341.

Pascual-Marqui, R.D., Lehmann, D., Koukkou, M., Kochi, K., Anderer, P., Saletu, B., Tanaka, H., Hirata, K., John, E.R., Prichep, L., Biscay-Lirio, R., Kinoshita, T., 2011. Assessing interactions in the brain with exact low-resolution electromagnetic tomography. Philos Trans A Math Phys Eng Sci 369, 3768–3784. doi:10.1098/rsta.2011.0081.

Pellegrini, F., Delorme, A., Nikulin, V., Haufe, S., 2023. Identifying good practices for detecting inter-regional linear functional connectivity from EEG. Neuroimage 277, 120218. doi:10.1016/j.neuroimage.2023.120218.

Peng, Y., Wang, J., Liu, Z., Zhong, L., Wen, X., Wang, P., Gong, X., Liu, H., 2022. The Application of Brain-Computer Interface in Upper Limb Dysfunction After Stroke: A Systematic Review and Meta-Analysis of Randomized Controlled Trials. Front Hum Neurosci 16, 798883. doi:10.3389/fnhum.2022.798883.

Pfurtscheller, G., Lopes da Silva, F.H., 1999. Event-related EEG/MEG synchronization and desynchronization: basic principles. Clin Neurophysiol 110, 1842–1857. doi:10.1016/s1388-2457(99)00141-8.

Pfurtscheller, G., Stancak, A.J., Neuper, C., 1996. Event-related synchronization (ERS) in the alpha band–an electrophysiological correlate of cortical idling: a review. Int J Psychophysiol 24, 39–46. doi:10.1016/s0167-8760(96)00066-9.

Pion-Tonachini, L., Kreutz-Delgado, K., Makeig, S., 2019. ICLabel: An automated electroencephalographic independent component classifier, dataset, and website. Neuroimage 198, 181–197. doi:10.1016/j.neuroimage.2019.05.026.

Popov, T., Tröndle, M., Baranczuk-Turska, Z., Pfeiffer, C., Haufe, S., Langer, N., 2023. Test-retest reliability of resting-state EEG in young and older adults. Psychophysiology 60, e14268. doi:10.1111/psyp.14268.

R Core Team, 2022. R: A Language and Environment for Statistical Computing. R Foundation for Statistical Computing. Vienna, Austria. URL: https://www.R-project.org/.

Ramoser, H., Müller-Gerking, J., Pfurtscheller, G., 2000. Optimal spatial filtering of single trial EEG during imagined hand movement. IEEE Trans Rehabil Eng 8, 441–446. doi:10.1109/86.895946.

Ritter, P., Moosmann, M., Villringer, A., 2009. Rolandic alpha and beta EEG rhythms' strengths are inversely related to fMRI-BOLD signal in primary somatosensory and motor cortex. Hum Brain Mapp 30, 1168–1187. doi:10.1002/hbm.20585.

Rubega, M., Carboni, M., Seeber, M., Pascucci, D., Tourbier, S., Toscano, G., Van Mierlo, P., Hagmann, P., Plomp, G., Vulliemoz, S., Michel, C.M., 2019. Estimating EEG Source Dipole Orientation Based on Singular-value Decomposition for Connectivity Analysis. Brain Topogr 32, 704–719. doi:10.1007/s10548-018-0691-2.

Samek, W., Blythe, D.A., Curio, G., Müller, K.R., Blankertz, B., Nikulin, V.V., 2016. Multi-scale temporal neural dynamics predict performance in a complex sensorimotor task. NeuroImage 141, 291–303. doi:10.1016/j.neuroimage.2016.06.056.

Sannelli, C., Vidaurre, C., Müller, K.R., Blankertz, B., 2019. A large scale screening study with a SMR-based BCI: Categorization of BCI users and differences in their SMR activity. PLoS One 14, e0207351. doi:10.1371/journal.pone.0207351.

Satterthwaite, F.E., 1946. An approximate distribution of estimates of variance components. Biometrics 2, 110–114. doi:10.2307/3002019.

Schalk, G., McFarland, D.J., Hinterberger, T., Birbaumer, N., Wolpaw, J.R., 2004. BCI2000: a general-purpose brain-computer interface (BCI) system. IEEE Trans Biomed Eng 51, 1034–1043. doi:10.1109/TBME.2004.827072.

Scherer, R., Vidaurre, C., 2018. Motor imagery based brain–computer interfaces, in: Smart Wheelchairs and Brain-Computer Interfaces. Elsevier, pp. 171–195. doi:10.1016/B978-0-12-812892-3.00008-X.

Schneider, M., Broggini, A.C., Dann, B., Tzanou, A., Uran, C., Sheshadri, S., Scherberger, H., Vinck, M., 2021. A mechanism for inter-areal coherence through communication based on connectivity and oscillatory power. Neuron 109, 4050–4067. doi:10.1016/j.neuron.2021.09.037.

Schoffelen, J.M., Gross, J., 2009. Source connectivity analysis with MEG and EEG. Hum Brain Mapp 30, 1857–1865. doi:10.1002/hbm.20745.

Shih, P.C., Steele, C.J., Nikulin, V.V., Gundlach, C., Kruse, J., Villringer, A., Sehm, B., 2021. Alpha and beta neural oscillations differentially reflect age-related differences in bilateral coordination. Neurobiol Aging 104, 82–91. doi:10.1016/j.neurobiolaging.2021.03.016.

Solodkin, A., Hlustik, P., Chen, E.E., Small, S.L., 2004. Fine modulation in network activation during motor execution and motor imagery. Cereb Cortex 14, 1246–1255. doi:10.1093/cercor/bhh086.

Steegen, S., Tuerlinckx, F., Gelman, A., Vanpaemel, W., 2016. Increasing transparency through a multiverse analysis. Perspectives on Psychological Science 11, 702–712. doi:10.1177/1745691616658637.

Stieger, J.R., Engel, S., Jiang, H., Cline, C.C., Kreitzer, M.J., He, B., 2020. Mindfulness Improves Brain–Computer Interface Performance by Increasing Control Over Neural Activity in the Alpha Band. Cerebral Cortex 31, 426–438. doi:10.1093/cercor/bhaa234.

Stieger, J.R., Engel, S.A., He, B., 2021. Continuous sensorimotor rhythm based brain computer interface learning in a large population. Sci Data 8, 98. doi:10.1038/s41597-021-00883-1.

Sugata, H., Hirata, M., Yanagisawa, T., Shayne, M., Matsushita, K., Goto, T., Yorifuji, S., Yoshimine, T., 2014. Alpha band functional connectivity correlates with the performance of brain-machine interfaces to decode real and imagined movements. Front Hum Neurosci 8, 620. doi:10.3389/fnhum.2014.00620.

Tadel, F., Baillet, S., Mosher, J.C., Pantazis, D., Leahy, R.M., 2011. Brainstorm: a user-friendly application for MEG/EEG analysis. Comput Intell Neurosci 2011, 879716. doi:10.1155/2011/879716.

Tao, X., Yi, W., Wang, K., He, F., Qi, H., 2021. Inter-stimulus phase coherence in steady-state somatosensory evoked potentials and its application in improving the performance of single-channel MI-BCI. J Neural Eng 18. doi:10.1088/1741-2552/ac0767.

Van Veen, B., Van Drongelen, W., Yuchtman, M., Suzuki, A., 1997. Localization of brain electrical activity via linearly constrained minimum variance spatial filtering. IEEE Transactions on Biomedical Engineering 44, 867–880. doi:10.1109/10.623056.

Vidaurre, C., Haufe, S., Jorajuría, T., Müller, K.R., Nikulin, V.V., 2020. Sensorimotor functional connectivity: A neurophysiological factor related to BCI performance. Frontiers in Neuroscience 14. doi:10.3389/fnins.2020.575081.

Wolpaw, J.R., Birbaumer, N., McFarland, D.J., Pfurtscheller, G., Vaughan, T.M., 2002. Brain-computer interfaces for communication and control. Clin Neurophysiol 113, 767–791. doi:10.1016/s1388-2457(02)00057-3.

Yuan, H., He, B., 2014. Brain-computer interfaces using sensorimotor rhythms: current state and future perspectives. IEEE Trans Biomed Eng 61, 1425–1435. doi:10.1109/TBME.2014.2312397.

Yuan, H., Liu, T., Szarkowski, R., Rios, C., Ashe, J., He, B., 2010. Negative covariation between task-related responses in alpha/beta-band activity and BOLD in human sensorimotor cortex: an EEG and fMRI study of motor imagery and movements. Neuroimage 49, 2596–2606. doi:10.1016/j.neuroimage.2009.10.028.

Zhang, R., Xu, P., Chen, R., Li, F., Guo, L., Li, P., Zhang, T., Yao, D., 2015. Predicting Inter-session Performance of SMR-Based Brain-Computer Interface Using the Spectral Entropy of Resting-State EEG. Brain Topogr 28, 680–690. doi:10.1007/s10548-015-0429-3.

Zoefel, B., Huster, R.J., Herrmann, C.S., 2011. Neurofeedback training of the upper alpha frequency band in EEG improves cognitive performance. Neuroimage 54, 1427–1431. doi:10.1016/j.neuroimage.2010.08.078.